

Implementation of a Hardware-in-the-Loop System Using Scale Model Hardware for Hybrid Electric Vehicle Development

Thesis submitted to the faculty of the Virginia Polytechnic Institute and State University
in partial fulfillment of the requirements for the degree of

Master of Science
In
Mechanical Engineering

John J. Janczak

Committee:
Dr. Douglas Nelson
Dr. Scott Huxtable
Dr. Al Kornhauser

June 28, 2007
Blacksburg, Virginia

Keywords: Hybrid, Hardware-in-the-Loop, HIL, Labview, control strategy

Copyright 2007, John J. Janczak

Implementation of a Hardware-in-the-Loop System Using Scale Model Hardware for Hybrid Electric Vehicle Development

John J. Janczak

Abstract

Hardware-in-a-loop (HIL) testing and simulation for components and control strategies can reduce both time and cost of development. HIL testing focuses on one component or control system rather than the entire vehicle. The rest of the system is simulated by computer systems which use real time data acquisition systems to read outputs and respond like the systems in the actual vehicle would respond. The hardware for the system is on a scaled-down level to save both time and money during testing.

The system designed to simulate the REV_{LSE} Equinox split parallel hybrid consists of five direct current (DC) permanent magnet motors. These motors are used in the system to test the controller software of the vehicle. Two of the motors act as power plants simulating the spark ignited Ethanol engine and the rear traction motor. These two motors are controlled by DC variable speed controllers. The other motors are used as generators to simulate the load from the belted alternator starter (BAS) and the road load on each axle. The motors on each axle are joined together mechanically using a belt and pulley system. The front and rear axle of the system are not connected to simulate the actual vehicle where the power plants are gear-reduced before they make contact with the road and therefore do not actually spin at the same speeds.

The computer software and hardware used to run the HIL hybrid system is National Instruments LabView and CompactRIO. LabView provides an easy interface through which programs for the RIO can be written. The RIO gives the user the ability to measure the power into and out of different components in the system to measure the efficiency of the system. The ability to measure system efficiencies using different powertrain inputs and loading schemes is what makes the HIL system a valuable tool in control modeling for the Equinox. LabView and the RIO allow the user to optimize the control strategy with the two power plant inputs and the BAS to make sure the high voltage system stays charged and improve the overall efficiency of the vehicle without the actual vehicle. The HIL system allows other work to be done of the vehicle during the control development.

During a constant axle speed test at 730 RPM with constant generator resistance, the front engine efficiency was 33.8%, the BAS efficiency was 53.0%, the rear load generator efficiency was 51.2% and the overall efficiency of the front axle was 24.0%. These results show that the system can simulate the powertrain of a hybrid vehicle and help create and validate a control scheme.

Acknowledgements

I would like to express my gratitude to Dr. Doug Nelson for his insight, support, and guidance through this project.

Table of Contents

1. Introduction.....	1
1.1 The Purpose of hardware-in-the-loop systems.....	1
1.2 Hybrid specific HIL testing.....	2
1.3 Research Objectives.....	5
2. Review of Literature.....	7
2.1 Hybrid HIL for combustion engine.....	7
2.2 HIL software issues.....	8
2.3 Advantages of a HIL system.....	9
2.4 Literature Review Conclusions.....	10
3. Component Selection.....	11
3.1 Computer Interface.....	11
3.2 Motors.....	14
3.3 Controllers.....	16
3.4 Load Generators.....	17
4. Scaled Down Hardware.....	19
4.1 Frame.....	19
4.2 Current Measurement Devices.....	20
4.3 Tachometer.....	23
4.4 Accessories.....	23
5. HIL Scaled Down Control Strategy.....	24
6. Instrumentation.....	30
7. Test Procedure.....	32
7.1 Powertrain Motors.....	32
7.2 Load Motors.....	35
7.3 Controllers.....	36
7.4 Mechanical Losses.....	38
7.5 Overall Axle.....	39
7.6 Limitations.....	39
7.6.1 Use of DC motors.....	39
7.6.2 Regenerative Energy Capture.....	40
7.6.3 Speed Sensing.....	40
8. Test Results.....	41
8.1 Drive Cycle Creation.....	41
8.2 Simple Drive Cycle.....	43
8.3 Complex Drive Cycle.....	45
9. Future Research.....	47
10. Conclusion.....	49
References.....	50
Appendix.....	51

List of Multimedia Objects

Tables

Table 1	Specifications for Moog C34-I70-20 Permanent Magnet DC motor.....	15
Table 2	Specifications for Dart 65 E10 DC Controller.....	17
Table 3	Tests were run to help understand the magnitude of HIL system mechanical losses.....	38
Table A-1	Cost and contact/ordering info for parts.....	52
Table A-2	Data collected from controller efficiency tests.....	53
Table A-3	Speed versus power measurements for motors.....	53

Figures

Figure 1	General configuration of a parallel through the road hybrid vehicle.....	2
Figure 2	General configuration of a series hybrid vehicle	3
Figure 3	General configuration of a split parallel architecture (SPA) hybrid vehicle.....	4
Figure 4	Example of FPGA code and user interface for outputting a voltage with a Compact RIO controller	12
Figure 5	Example of the real time portion of the LabView code	13
Figure 6	Example of the real time user interface in LabView	14
Figure 7	Moog C34-L-70-20 Permanent Magnet DC motors were used both as power plants and generators.....	16
Figure 8	Ohmite power resistors are used to generate a resistance to the powertrain motors.....	18
Figure 9	T-SLOTS aluminum extrusion was used as a frame for the system	20
Figure 10	Shunt resistors are used to measure the current draw through various components of the system.....	21
Figure 11	Current transducers are used to measure the current flowing through the motors from the motor controller PWM signal	22
Figure 12	The powertrain and load component distribution of an actual hybrid vehicle	25
Figure 13	The HIL system configuration which simulates the powertrain components and various loads on a hybrid vehicle.....	25
Figure 14	Relationship of velocity to power consumed by a vehicle.....	28
Figure 15	The relationship between motor speed and power of a generator for a fixed load resistance of 5 ohms.....	28
Figure 16	Schematic of the electrical and mechanical connections of the HIL system	31
Figure 17	Diagram of DV_{PT} in equation 7.....	33
Figure 18	Efficiency map of the Dart controllers as a function of I^2	37

Figure 19	Example of the programming code used to create a predetermined drive cycle in LabView	42
Figure 20	Simple drive cycle used to test and validate the HIL system	43
Figure 21	Power and efficiency outputs during the simple drive cycle at full speed	44
Figure 22	Example of a more complex drive cycle that can be simulated using the HIL system	46
Figure A-1	Complete specifications list for Moog motors.....	51
Figure A-2	Complete specifications for Dart controllers.....	52

Equations

Equation 1	Resistance	18
Equation 2	Aerodynamic drag	26
Equation 3	Inertial Force.....	26
Equation 4	Rolling Resistance Force.....	26
Equation 5	Power relation.....	27
Equation 6	Motor Power	27
Equation 7	New resistance form	27
Equation 8	Vsupply.....	32
Equation 9	dV	33
Equation 10	Power output for motor.....	33
Equation 11	Power input for motor	34
Equation 12	Torque input for motor.....	34
Equation 13	Torque output for motor.....	34
Equation 14	Alternate motor power output	34
Equation 15	Motor efficiency.....	34
Equation 16	Power output for generator.....	35
Equation 17	Torque input for generator.....	35
Equation 18	Speed conversion	35
Equation 19	Power input for generator.....	36
Equation 20	Efficiency of generator	36
Equation 21	Power into controller.....	36
Equation 22	Efficiency of controller.....	37
Equation 23	Overall axle efficiency.....	39

Abbreviations

Ω	Ohms
A	Amperes
AC	Alternating current
BAS	Belted alternator starter
DC	Direct current
DFMEA	Design failure modes and effects analysis
ECU	Electronic control unit
FPGA	Field-programmable gate array
HEVT	Hybrid Electric Vehicle Team
HIL	Hardware-in-the-loop
mV	Millivolt
Nm	Newton meter
PAC	Programmable automation controller
PSAT	Powertrain system analysis toolkit
PWM	Pulse width modulation
RMS	Root mean square
RPM	Revolutions per minute
RTM	Rear traction motor
SIT	Simulation interface toolkit
SOC	State of charge
SPA	Split parallel architecture
V	Volts
W	Watts

1. Introduction

1.1 The purpose of Hardware-in-the-loop systems

Today's vehicles are becoming increasingly complex. As carmakers try to succeed in a very competitive industry, they introduce new and sophisticated features to differentiate their products from the products of their competitors. More stringent regulations on vehicle fuel economy and emissions also require additional control and monitoring systems to the electronic control units (ECU's) of vehicles. This trend is becoming increasingly important in the world of hybrid vehicles. The control systems in these vehicles are very complex and finely tuned to maximize the efficiency of the vehicles. Testing these new systems can be extremely time consuming and expensive for carmakers in an industry where development time and cost are the key factors for bringing innovations to the marketplace.

Hardware-in-the-Loop (HIL) testing and simulation for various components and control systems of vehicles can prove to be quite time and cost efficient for carmakers. Instead of testing an entire vehicle, HIL testing consists of one component or a group of components from a system with computer simulated inputs that represent the rest of the vehicle or system. The inputs to the component(s) act as inputs the component(s) would read from other systems or components in a real vehicle. Real-time sensors and data acquisition systems are then used to acquire the output from the component being tested. Testing in this manner can greatly reduce test time, cost of testing and testing space. The signals usually generated by multiple systems of a vehicle can all be generated by one computer so an entire vehicle body is not needed to test one component of a system. HIL testing saves the developer money by allowing a single simulation system to emulate multiple input signals that would otherwise come from a plethora of other systems in the vehicle which would cost much more money and time to produce. The computer simulated signals can easily be changed to conduct multiple tests with one HIL setup. HIL testing can be done either at a full-scale level with actual components or on a scaled-down level. HIL testing on a scaled down level can save space and money on the basis of testing a system where all of the parts are equally scaled to a smaller size so the system still runs as it would at the actual full-scale level. This can be a very effective modeling approach for vehicles because powertrain components can be very bulky and expensive.

1.2 Hybrid Specific HIL Testing

Even though there are countless numbers of hybrid vehicle designs floating around today, they all stem from a few general architectures or powertrain configurations. The two main hybrid vehicle architectures are parallel and series. Since the HIL model is capable of simulating each of these architectures with slight manipulation of the components, each of the architectures will be introduced below. A parallel architecture, as seen in Figure 1, consists of a separate power plant on each axle of the vehicle [1]. In most cases, the front axle is either powered by a fuel cell or internal combustion engine which acts through a transmission to power the axle. The rear axle can be powered by an electric motor or fuel cell which runs from a high voltage battery pack or hydrogen tank in the vehicle. The battery pack may be recharged by plugging into the power grid, or by the use of regenerative braking which uses the inertia of the vehicle to recapture power while the vehicle's brakes are being applied. The electric motor on the rear axle can also extract power from the front axle (in a negative torque mode) in order to recharge the battery pack.

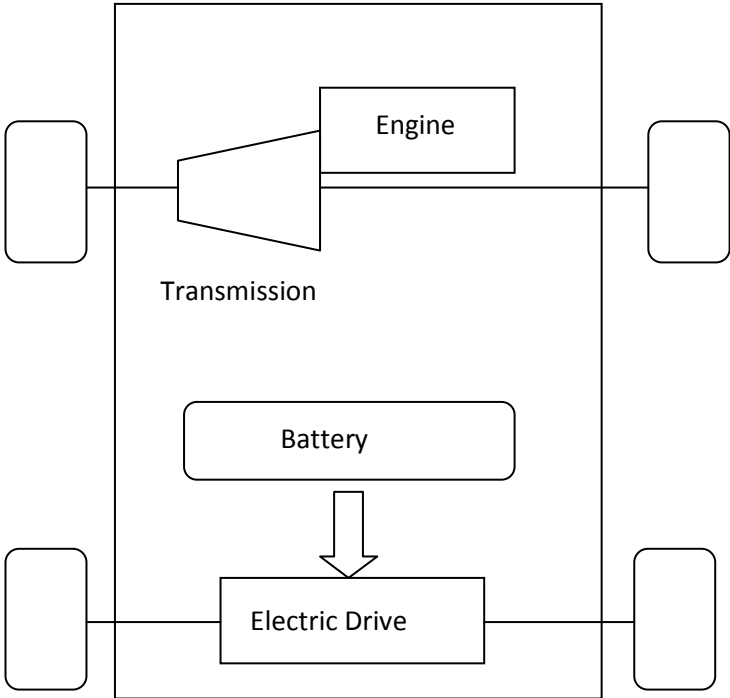


Figure 1. General configuration of a parallel through the road hybrid vehicle.

The second major architecture for hybrid vehicles is the series architecture as seen in Figure 2 [1]. In a series hybrid vehicle, two or more power plants work in series to power the vehicle. The power generally is supplied to one axle. An example of this

would be an internal combustion engine coupled with a generator that could either provide energy to the battery pack, or help drive an electric motor [5]. The electric motor would be the only source of motion for the vehicle. In this case, the engine could almost always run at its most efficient points and the energy produced when the vehicle is decelerating or stopped can be used to recharge the battery pack.

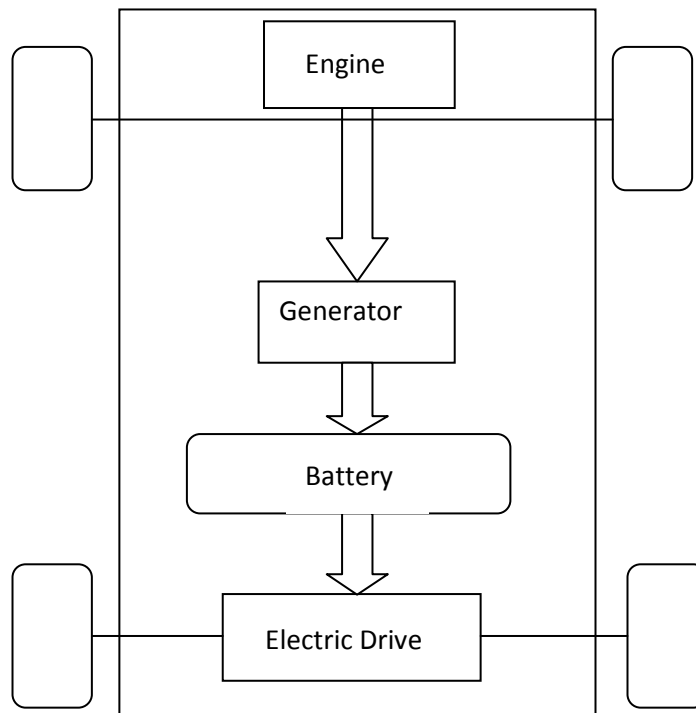


Figure 2. General configuration of a series hybrid vehicle

A third architecture, which can be seen in Figure 3, and is the architecture of the hybrid vehicle this HIL system was originally modeled after, is a combination of a parallel and series hybrid architecture which is referred to as split-parallel architecture (SPA) [1],[5]. This is the current architecture employed in the vehicle of the members of the Hybrid Electric Vehicle Team (HEVT) at Virginia Tech, and is the reason the HIL system was configured this way. This setup uses a belted alternator starter (BAS). The BAS has two main purposes. It can act as a high voltage alternator for the system in which case it can be used to load an internal combustion engine on the front axle of the vehicle. This in turn allows the control system to run the engine at its most efficient points which can be determined by mapping the engine performance. While the BAS is loading the engine, it is producing negative torque which can be used to charge a high

voltage battery pack. In this case, the battery pack powers a rear traction motor which is the power plant on the rear axle of the vehicle. The other use of the BAS in a SPA architecture is for quick engine start. The internal combustion engine on the front axle can be turned off when it is not needed. These cases would be while the car is idling, braking, coasting, or in electric only mode. When additional power is needed by the front axle, the BAS acts as an instantaneous starter for the engine even if the car is in motion and the engine can drive the front axle to the desired speed or torque demanded by the driver.

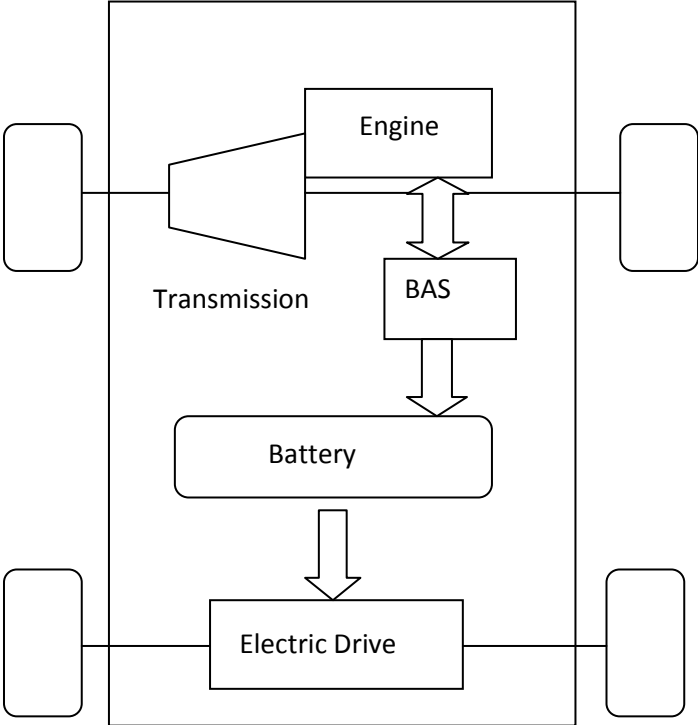


Figure 3. General configuration of a split parallel architecture (SPA) hybrid vehicle

Even though there are two or three main architectures for hybrid vehicles, there are numerous configurations and components that can be used with each of them. As stated in the above descriptions, different power plants can be used including fuel cells, gasoline, diesel, biodiesel, ethanol or hydrogen combustion engines, or electric drives. This is where HIL simulation for hybrid vehicles becomes advantageous. The modeling and control strategies for these vehicles can be done on a scaled-down level with cheaper and more versatile components. Single motors can be used with computer software to emulate any of the several different power plants mentioned above. The

components can easily be reconfigured from one architecture or control strategy to another. This easy reconfiguration could reduce various stages of testing cycles and therefore reduce testing time as a whole. Driver inputs, various driving conditions, and validated components can all be computer-simulated. Components can be tested on multiple drive cycles without ever touching a road which gives the researcher a much safer way to validate the control strategy behavior of a system. Another reason to use HIL simulation testing on newer technology such as hybrid vehicles is to save the expense of damaging expensive components during testing. This includes testing, verifying and expanding the design failure modes and effects analysis (DFMEA) before the systems are implemented on the actual vehicle. New control strategies and system components in some hybrid vehicles are pushing the envelope to achieve higher and higher efficiencies with less emission output, which means some components will be pushed to their limit. If this can be done on a smaller-scale, less expensive level, it can save development businesses significant resources.

1.3 Research Objectives

The main objectives of this research are first to build a scaled-down model of the powertrain of the split parallel hybrid HEVT REV_{LSE} Equinox at Virginia Tech which can be used for testing the controls system of the vehicle on a much smaller level, and correspond the model to a data collection system which can analyze the data. The components and controller of the system should simulate the actual powertrain components and controller on the vehicle for accurate results. The purpose of such a system is to develop and validate a control strategy for the vehicle without the use of the hard to replace and expensive components used on the vehicle. The HIL system also allows other work and tests to be run on the vehicle while the controls testing is taking place. The model should run through a computer interface which is intuitive to use and changes dynamically along with the system.

The following chapters in this thesis will start with the chapter 2, which is a review of literature of prior HIL systems built for slightly different purposes along with their successes and troubleshooting advice. Chapter 3 consists of an in-depth component analysis which explains the criteria and specifications for selection of the system's computer interface, motors, controllers, and load generators on the HIL system. The fourth chapter describes the need and selection criteria for the hardware of the system including the frame, current measurement devices, tachometer, and system accessories. Chapter 5 explains the control strategy of the scaled-down HIL system. This relates the model to the vehicle in terms of load and power from each of the

components as well as load and power variability as it relates to vehicle speed. Chapter 6 introduces the mechanical makeup and a schematic of the HIL system. Chapter 7 is a detailed section on the test procedure of the HIL system including the calculations of load, power, torque and efficiencies of each component as well as the efficiency of the overall system. This chapter also includes the limitations of the system and possible solutions for each of the limitations. Chapter 8 verifies the functionality of the system and shows results from two different drive cycles created with LabView. The drive cycles and resulting data indicate the usefulness of the system in creating a control strategy for a hybrid vehicle. Chapter 9 indicates future research and improvements for the system which can be carried out by another graduate student. Chapter 9 gives the conclusions of the research which relates the results of the system to the original objectives set forth at the beginning of the project.

2. Review of Literature

As interest in hybrid electric vehicles continues to grow, more research is being conducted on their components and control systems. This research consists of software modeling, full-scale hardware-in-the-loop modeling, and scaled-down hardware-in-the-loop modeling. This section contains a brief summary of HIL research and modeling conducted in the past by other research facilities.

2.1 Hybrid HIL for combustion engine

In 2007, Winkler and Guhmann [2] designed a full-scale hardware-in-the-loop test stand for a combustion engine which was coupled with a dynamometer. The modeling system used to analyze the outputs from the HIL system was Modelica. The rest of the hybrid system was modeled using I/O cards and real-time computer simulation. This included the clutches, transmission, and electric motors. The use of the software allowed Winkler flexibility with the hybrid components of his system. With the computer, he could easily change their locations in the system as well as their efficiency characteristics. In the paper, it is stated, "The use of HiL simulations in connection with engine test-benches allows us to obtain very accurate predictions [of] the exhaust-gas emissions and fuel consumption in an early phase of the development process." The original powertrain tested on this bench consisted of the engine, a starter/generator/battery, and the transmission, but also accounted for clutch and drive line losses. The HIL system was used along with efficiency models of the simulated parts to develop a control strategy which provided the best fuel economy by using the engine and generator in the ranges which they provided the best efficiency for the overall vehicle. The control strategy has the ability to keep the state of charge (SOC) of the battery at reasonable levels and can determine when it more efficient to use the electric motor to assist the vehicle rather than loading the engine to recharge the battery. Another test Winkler performed with his bench was to use both a first and second order polynomial system to model the battery charge/discharge sensitivity curve. The sensitivity curve determines the charge/discharge rate of the battery by the SOC. For example, when the SOC reaches its upper or lower limit, the sensitivity curve allows it to charge/discharge at a faster rate than when it is in the acceptable range. He concluded that a second order polynomial model does not allow the battery to discharge as quickly as a linear model.

2.2 HIL software issues

In 2003, Dynasim, a Swedish company, published a paper [3] about its new HIL modeling software. The portion of the paper that is of interest describes some of the main difficulties of using software in order to model the missing components of a HIL system, and choosing the complexity of the software model. The paper starts out by describing some problems that people can run into during the use of software for HIL system modeling. One of the first problems addressed in and throughout the paper is the speed of the computer used to simulate and record system data. In the case of full control systems, the computer might not have the capability to sample at least as fast as the electronic control unit (ECU) of the vehicle to ensure real-time data. In most cases, it is preferred to sample at a faster rate than that of the ECU. A second major issue in HIL modeling is the accuracy at which very low angular velocities can be measured. Angular velocities are very important in multiple aspects of HIL testing including torque calculations and ECU control strategy. The paper also adds event propagation as a HIL software modeling problem. This basically includes a mistake in one of the simulated components may carry over and cause other components to work incorrectly or falsely meet specifications. The paper also discusses modeling a sedan chassis at different levels of complexity. Each level accounts for a greater level of detail of the system. For example, the first level, which uses 15 degrees of freedom, models the suspension by using tables of polynomials while the fourth model, which uses 72 degrees of freedom, includes the suspension with linkages joined by bushings where mass and inertia of the bar are taken into account. There were improvements from the polynomial tables compared to the whole suspension model, but once the main components (linkages and bushings) were accounted for, which left out the small mass and inertia of the bar connecting them, the improvement in the models did not outweigh all of the extra degrees of freedom and extra equations needed to construct the model. This paper is useful in determining the complexity of the HIL system used to simulate the HEVT vehicle. It points out calculations that are difficult to simulate such as velocity and torque. The complexity of the system increases the work done both by the Compact Rio and by the computer that is used to run the interface. The system needs to run at a certain complexity to acquire somewhat reasonable results, but there is a point where extra complexity is unnecessary and does not significantly impact the results of the model.

2.3 Advantages of a HIL system

Abdourida et al. published a paper discussing the design and testing of HIL systems for electric drives [4]. They begin explaining the reasoning behind HIL simulation versus non-real-time simulation followed by actual system testing. The reasons given include the troubles caused by transition from non-real-time simulation to actual prototype testing along with the time the simulation takes for complex systems. HIL also alleviates the struggles of assembling a complete system in order to test one component of the system especially if the testing is to be conducted on an existing system which is already in place. Such assembly can be both expensive and time consuming. Using HIL simulation can shorten the iteration process for developing and verifying motor drives systems. The simulation also greatly reduces the amount of hand code that goes into the testing resulting again in shorter development times, but also eliminating errors in the coding. The paper states, "Hardware-in-the-Loop simulation permits repetition and variation of tests on the actual or prototyped hardware without any risk for people or the system." In the case of testing motor drives, HIL can be used to either simulate the entire system in real-time or test one component of the system modeling the rest of the system in real-time. Multiple systems can be modeled together to form a single system for production. The example they give is testing an inverter and traction motor and DC-DC and AC-DC converters for a hybrid vehicle. The last reason the paper gives for HIL testing is "the tests can be performed under realistic and reproducible conditions...and programmed and automatically executed." The testing of an electronics system usually consists of a controller and a plant or motor which are assembled in a loop which uses feedback to instruct the controller. The use of HIL simulation consists of using a computer program such as Simulink to design a block diagram for the system and then letting Simulink generate the necessary code to run the simulation. Once the code is generated, the controller, the motor drive, or both can be validated using as much actual hardware as desired and the rest can be simulated using a computer. The paper states that in the case of testing power electronic systems, computer speed becomes an issue. Testing systems with inputs and outputs that vary quicker than the sampling rate of the acquisition system and computer can cause problems such as spurious voltage spikes and non-linearity of the controllers. The solution so far is to use an interpolation algorithm such as RT-LAB to determine the time change and accurately simulate such events. In the case of controllers using PWM signals, computers cannot yet sample fast enough to accurately read the signals. The signals must be read using an FPGA board which boasts a high speed clock, which can then be relayed to the acquisition system on the computer. In the cases when the simulation becomes too complex for the computer to process, computers can be used in parallel in order to handle the load of the simulation system. This paper explains the

necessity of a HIL system for component testing. It explains many of the same benefits as the introduction to this paper about HIL simulation. It also shows a need for a real-time controller along with an FPGA computer interface to attain reasonable results from the system.

2.4 Literature Review Conclusions

Each of the above papers thoroughly explained the HIL system created for a particular purpose. The papers show reasons for implementation of certain hardware and software along with troubleshooting tips and solutions to problems that are usually run into while building a HIL system. While building a new HIL system, certain mistakes can be avoided due to the knowledge of the previous systems, along with keeping in mind that each system is also unique. None of the researched HIL systems are built for the same purpose or using the same components as the system discussed in this paper, so even though my research builds on previous work, it is a unique system with different components and control strategies of any of the researched models. This indicates that the literature review is helpful to a certain point, but trial and error testing will most likely have to be performed on the system.

The following chapter discusses the selection criteria and specifications for the major components of the system including the computer interface, motors, controllers and load generators for the HIL system. The component selection is crucial for developing a system that works properly together.

3. Component Selection

As previously noted, in using a scaled-down HIL system, the same system can be used to model any of the hybrid architectures relatively easily. The flexibility of the system needs to be considered during component selection. The number and type of components used in the HIL system must satisfy the basic requirements of each architecture and configuration. The SPA architecture has both the most components and most complexity. Therefore the component selection was largely based on that architecture. The major components needed for the construction of the HIL system are the computer interface, motors, controllers, and load generators. The selection criterion for each component is discussed below in its own self titled section.

3.1 Computer Interface

The computer interface is crucial for the effectiveness of a HIL system. The interface must accurately simulate output signals as well as accurately read input signals from the HIL simulation hardware. The interface must also be able to manipulate data in order to attain useful information from the system. The majority of the time, the information gathered by the computer interface is run through a secondary program for analysis. For example, data from a vehicle gathered by an interface can be analyzed using the Powertrain System Analysis Toolkit (PSAT) to simulate running the vehicle in different conditions or on different drive cycles.

In order to most accurately simulate the actual control system of the vehicle being modeled, the computer interface used in the vehicle was also chosen to use in the HIL system. The higher level control system of the actual vehicle is based on using MATLAB and Simulink so the code can be tested in PSAT and directly implemented into the vehicle. Simulink reads the power demand input from the driver and meets that demand using the vehicles most efficient state or most efficient component selection for that demand. The Simulink code is read in through the primary control hardware, the CompactRIO and LabView, using Simulation Interface Toolkit (SIT). Both the vehicle and HIL system contain a National Instruments CompactRIO programmable automation controller (PAC). LabView, via the CompactRIO, is used for control and communication with the individual components of the vehicle and HIL system. The CompactRIO can be used both as a real time controller and a data acquisition system which is extremely useful in this application. The use of Simulink is bypassed in the HIL model and can be input into the LabView interface of the RIO in its place. The system alone is not complex enough for the use of Simulink. The RIO in the HIL system holds up to four hot

swappable I/O modules which are individually designed for a specific type of signal. The modules used in this particular control system are a 10 volt output, a 60 volt input, and an 80 millivolt input. The RIO also has an embedded field programmable gate array (FPGA) chip which is used in conjunction with LabView. An FPGA program is written in LabView and then downloaded to the RIO using a crossover cable. The FPGA code used for the control system of the HIL model is relatively simple as seen in Figure 4. Figure 4 is the FPGA code and user interface for the voltage output portion of the RIO. The voltage output channel is placed within a while loop. The loop runs continuously until the stop button on the user interface portion below is depressed. The dial is used to communicate with the RIO what voltage to output. The value on the dial is in bits, which is converted to a voltage in the real-time portion of the program.

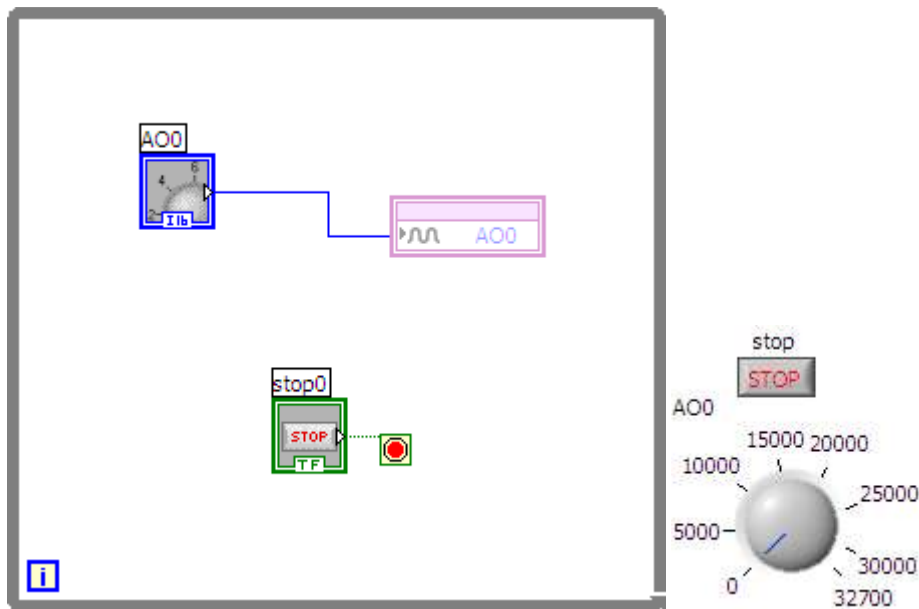


Figure 4. Example of FPGA code and user interface for outputting a voltage with a CompactRIO controller.

In addition to using FPGA programming to run the HIL system, real time programming is also used. The real time programming is used to ensure that the RIO processes the requests to it in a certain amount of time. The real time code actually reads in the FPGA code to another while loop and uses it as seen in Figure 5.

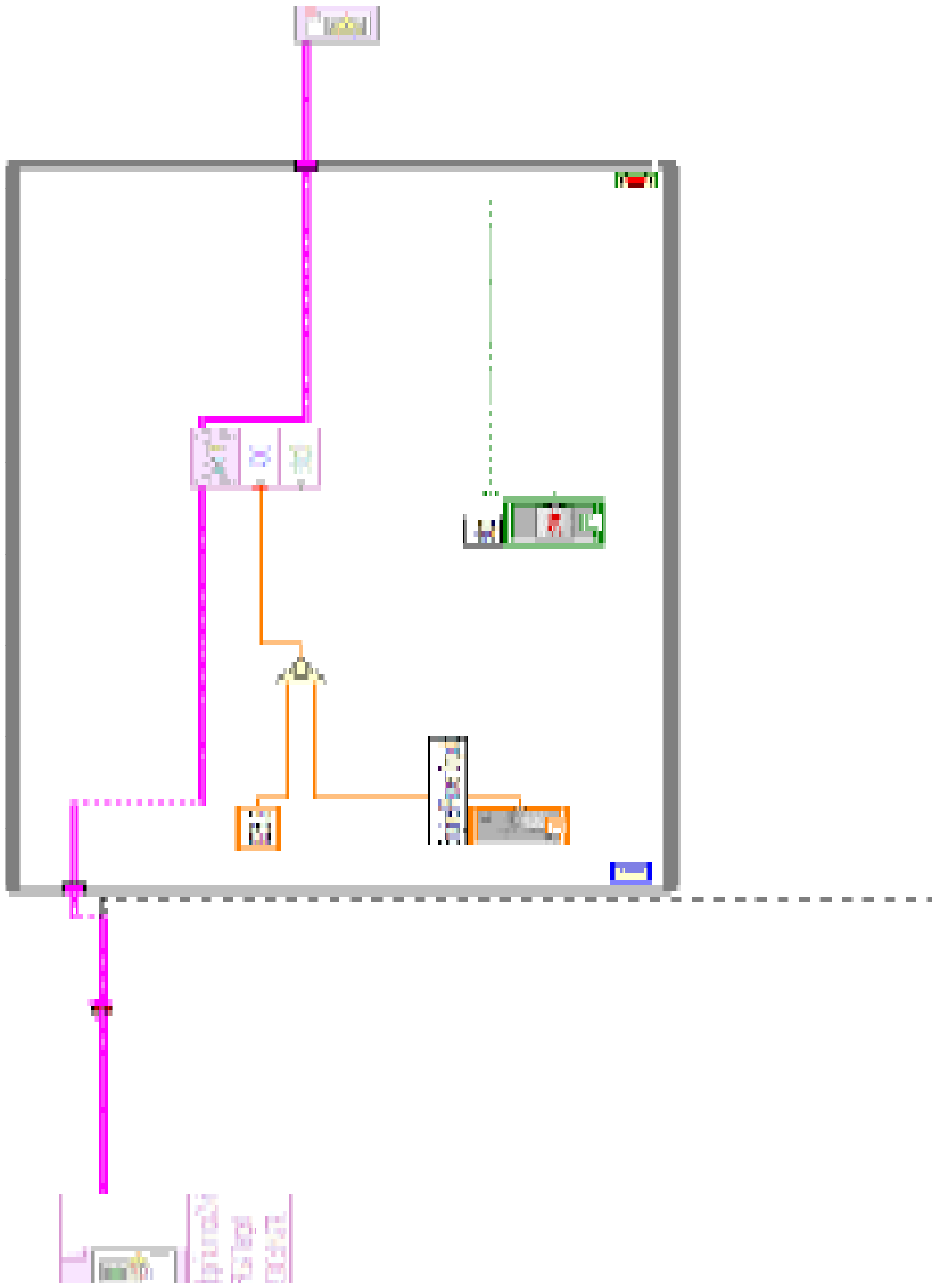


Figure 5. Example of the real time portion of the LabView code.

The real time code reads in the FPGA portion of the code through the block on the far left. As shown, the code is then converted from bit form to voltage form. The next step is to run the input through the processor and then the code runs back out of the while loop and terminates on the far right. This process continuously takes place until the stop button on the user interface is depressed. The output voltage, input voltage, current, and power portion of the user interface for one of the motors is shown in Figure 6.

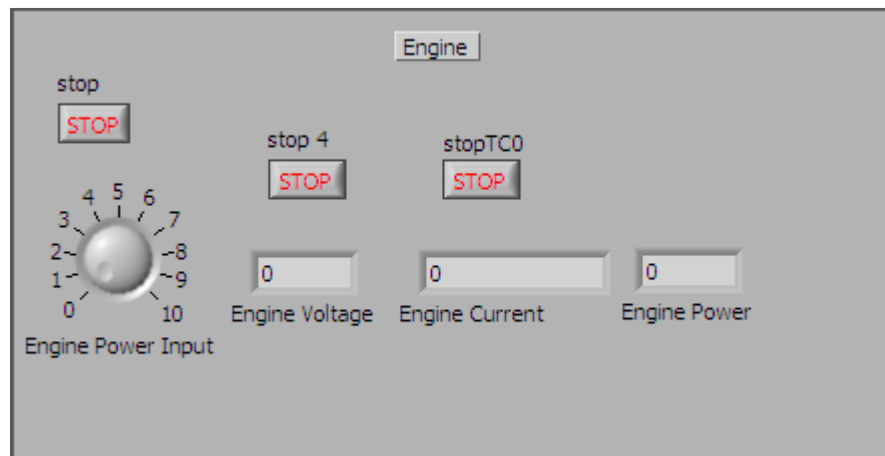


Figure 6. Example of the real time user interface in LabView.

This is a portion the actual interface used to run the HIL system. LabView helps to create a user friendly interface that does not require a vast amount of computer knowledge to run. Figure 6 shows how the HIL system can be manipulated manually to adjust the output of the powertrain motors in the system. The vehicle models eventually created for testing on the system can be implemented using drive cycles for each of the powertrain motors to determine the most efficient state of the entire system at different driving conditions. The creation and implementation of drive cycles for this system is further detailed in Chapter 8.

3.2 Motors

The motor selection for the HIL system was critical. The motors must be able to simulate multiple powertrain items mentioned previously in the section explaining different hybrid architectures. A direct current (DC) brushed permanent magnet motor

from Moog (C34-L70-20) was chosen as seen in Figure 7. The specifications for the motor are shown below in Table 1 and will be discussed in this section. The motors are all identical so they can be swapped out in place of each other and to reduce the complexity of the system. The cost and contact info for the components listed in this paper can be found in Table A-1 in the Appendix. The complete list of specifications for the motors can be seen in the Appendix Figure A-1.

Table 1. Specifications for the Moog C34-L70-20 Permanent Magnet DC motor	
Voltage (volts)	24-36
Rated current (amps)	7
Rated power (watts)	221
Rated speed (RPM)	2720
Peak Torque (Nm)	6.04
Rated Torque (Nm)	0.78
Weight (kg)	3.63

The initial idea for the system is to run off batteries, so the system is easily transportable. The options are then to use alternating current (AC) motors and a converter or to use direct current (DC) motors. Using DC motors was chosen to keep the complexity of the system down as far as possible. The decision to use brushed motors was made based on the fact that brushless permanent magnet motors are usually speed controlled and require a three phase input. The controller for brushless motors is also more expensive and more complicated, whereas a brushed motor controller is just a simple pulse-width modulation (PWM) controller. The motor is controlled by the voltage input. The current and speed of the motor are a function of the voltage input and load on the motor. The brushes and commutators somewhat limit the rated speed for the motors. There is a trade-off between motor size (power) and speed. It is not desirable to have very high speed motors for the system. Generally smaller motors operate at higher speeds. Therefore the motor chosen has a higher rated power than absolutely necessary, but the rated speed is in a level that is not difficult to deal with or run belted systems. The rated current level of the motor has to correspond with the rated output current of the controller used to power the motor. If a motor with a high current is chosen then the controllers have to be rated to continuously output high current levels which can get expensive. The disadvantage of the larger, more powerful

motors is that the physical size and weight of the motors is an issue for the transportability of the system. A downside to the brushed motors is that you cannot dynamically control the motor as a generator, but the motor just goes into generation mode when the back EMF of the motor is larger than the voltage applied to the motor.

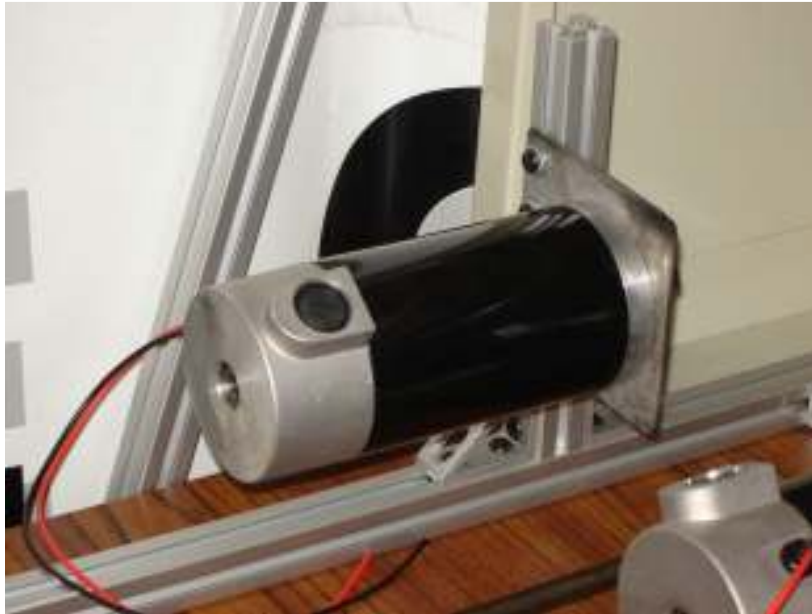


Figure 7. Moog C34-L70-20 Permanent Magnet DC motors were used both as power plants and generators.

3.3 Controllers

The controllers in the HIL system are used to vary the input voltage from the batteries to the motors. The motors selected are variable speed motors, so the controller does not specify the motor speed, but it specifies the voltage input to the motor and then depending on load, the corresponding input current and speed for the motors. Since the controllers were chosen after the motors, the controller selection was based completely on the Moog motors. The controllers used for the system are Dart Control 65E10 DC controllers. The specifications for the controllers are shown in Table 2. A complete list of the controller specifications can be seen in Figure A-2.

Table 2. Specifications for Dart 65E10 DC controller	
I/O Voltage (V)	24-36
Continuous current (A)	10
Speed adjustment	5K Ω potentiometer or 0-10 V DC

The input and output voltage for the controllers must match that of the motors. Since the motors are rated at 7 amps continuous, it is a benefit to use controllers with at least the same current rating or possibly a slightly higher current rating as to not overheat the controller. The natural convection, air cooled Dart controllers are rated at 10 amps continuous which is a good match for the motors. Another important specification considered during controller selection is the desire to adjust the controllers with LabView rather than a potentiometer. Most controllers are capable of this type of control due to the fact that a potentiometer uses a resistor to vary the voltage input to the speed adjustor of the controller, but it was important to find a controller that was in the 10 volt range and specified the possibility of a voltage input for speed control. A 10 volt input range was specified because of CompactRio module limitations. Currently a 10 volt output is the largest voltage module available for the Rio.

3.4 Load Generators

The last major component selection for the HIL system is load generators. Some of the motors in the system will act as powertrain components (engine, rear traction motor) and some will be used to load the powertrain components (BAS, front and rear axle load). The motors that will be acting as loads need some sort of component that will apply a reverse loading or negative torque on the system. Simply spinning the motors will only apply a load equal to the mechanical resistance of the motors. A voltage will occur but no current will run through the motor leads resulting in no power dissipation. Since the system is stationary, power resistors make the most sense. With the selection process narrowed to power resistors all that is left is to find resistors which match the motors and controllers already selected. This means finding a power resistor with both the correct resistance and power dissipation ability. Since the motors are rated at 221 watts and 7 amps, the power dissipation needed from a resistor can be found using the equation

$$R (\Omega) = \frac{P}{I^2} \quad (1)$$

Where R is the resistance of the load, P is the power dissipated and I is the current. The resultant resistance is 4.5 ohms. The Ohmite power resistors, seen in Figure 8, are rated at 5 ohms and 225 watts. They will be able to handle both any current level and power that one of the motors could supply.

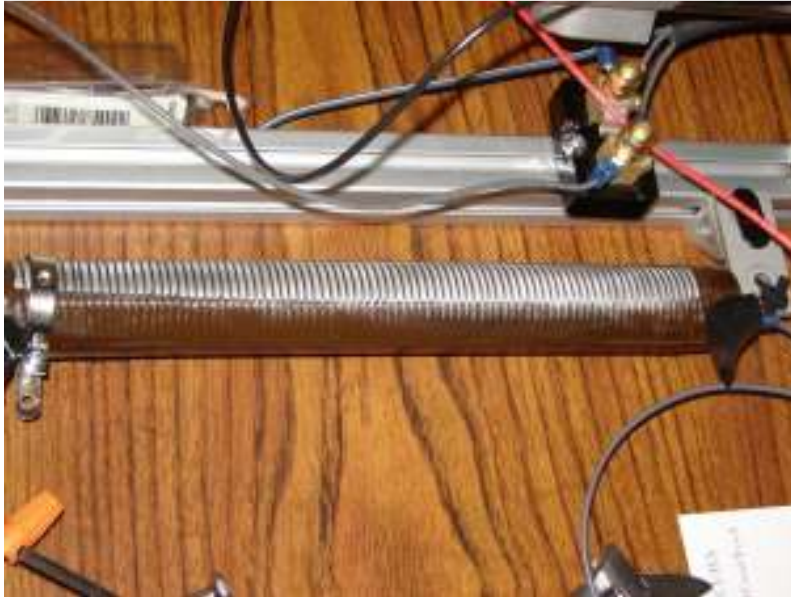


Figure 8. Ohmite power resistors are used to generate a resistance to the powertrain motors

Although not applicable to the current system due to cost constraints, when a controller with regeneration capabilities is used, the motor/generators such as the BAS, front load motor and rear load motor can be hooked up directly to the regenerating (two-quadrant) controller. The regenerative controller will capture the energy generated by the load motors and apply that energy to recharge the batteries. The use of a controller (rather than a resistor) here would allow control of the torque or resistance of the load generators as a function of speed to better represent the road load and inertia characteristics of a vehicle (see Chapter 5).

4. Scaled Down Hardware

In the previous section, there was a discussion on the component selection for the HIL system. This section describes the hardware necessary for the system to function properly. The hardware discussed includes the frame, shunt resistors, current transducers, speed sensors, belts, axles, and pulleys.

4.1 Frame

The frame used for the HIL system needs to be sturdy enough to support the motors and also the torque the motors can generate. Since the system will be used during competitions and for demonstrations, the frame needs to not only support the system, but also have a good look to it. For these reasons, aluminum extrusion frame was chosen from TSLOTS. Aluminum is not only lightweight, which is needed for a portable system, but also strong. The 1"x1" slot frame is very versatile which is ideal for trying to model multiple systems. The slot frame also included pieces which can hold the ball bearings used to allow rotation of the axles. The frame connects using T slots in the aluminum and hex head screws so no welding or joining of pieces is necessary which makes the frame look more professional. A picture of the frame can be seen in Figure 9.



Figure 9. T-SLOTS aluminum extrusion was used as a frame for the system

4.2 Current Measurement Devices

In order to correctly analyze the system for power, torque, and efficiency, the voltage as well as the current at certain nodes needs to be known. The PWM controllers are used to input a variable voltage to the driving motor, and from the load demanded, a certain current is necessary to drive the load. The same goes for the voltage produced through the load motors, where the current is determined by the voltage input and the value of the resistance. Even though the current is not specified or manually controlled, the value of the current is important. Two good ways to measure current include shunt resistors, as seen in Figure 10, and current transducers, as seen in Figure 11.

Shunt resistors are placed in series with the motor and resistors and output a voltage in millivolts which the CompactRIO can read and convert to a current reading. Shunt resistors are good candidates because they do not require external power, and they are accurate. The one downside is that they dissipate some voltage from the system, but the voltage they dissipate in this application is negligible (millivolts compared to 10-20 volts). The shunt resistors chosen are 100 amp to 100 mV resistors (CSA100-100). This means they can measure up to 100 amps accurately and each mV read across the resistor is representative of one amp. The reason for using a shunt with such a high current reading capability was due to the voltage output. The shunt resistors only dissipate one mV from the system per amp. Using a shunt resistor with a higher mV to amp output would dissipate much more voltage from the system. None of the components of the system are rated at more than 10 amps which ensures the shunt resistors can read any of the currents running through the system accurately, and at most will only dissipate 10 mV from the system at any given time.

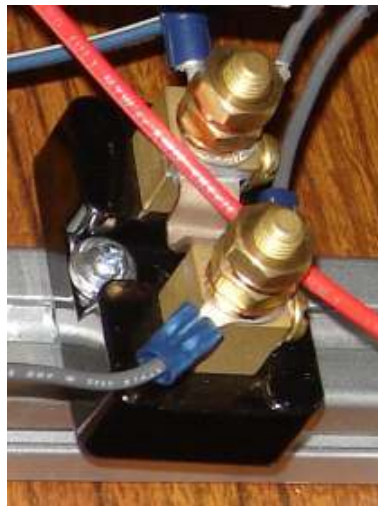


Figure 10. Shunt resistors are used to measure the current draw through various components of the system.

Current transducers are also a good tool used to read the current through a system. The transducers used in this system are Flex-Core H970LCB DC current transducers. These transducers use the Hall Effect, which utilizes a magnetic field, to report the current of the system. The transducers considered for this system, like the shunt resistors, report a voltage the CompactRIO which can then use the voltage to output a current measurement. The current transducers are valuable because they are non-intrusive to the system, meaning they do not directly connect to the system or draw any voltage loss. They have the potential to be just as accurate as a shunt resistor.

Current transducers also can output the current in terms of volts instead of millivolts which makes it easier for the RIO to accurately read the input. The downside to the current transducers is they are generally at least a factor of ten times more expensive than shunt resistors, and they also must be externally powered, usually at a different voltage than the motors, which makes for a more complex wiring system.



Figure 11. Current transducers are used to measure the current flowing through the motors from the motor controller PWM signal.

For the HIL system created here, both shunt resistors and current transducers are used. Shunt resistors are used in all of the applications except for the post-controller current reading due to their low cost and no powering requirements. When it comes to reading the current level on a PWM signal, the shunt resistor and RIO are not capable of giving an accurate RMS current reading of the system. A PWM signal switches the input voltage to the motor on and off at very high speeds to simulate certain reduced voltage inputs. For example, if a 24 volt source is connected to a PWM controller which is turned halfway up, the controller will apply the voltage as a square wave with the frequency and period such that a motor will respond as if it is receiving a 12 volt signal. The shunt resistor will then provide the RIO with segments of the wave depending on the sampling frequency of the RIO. The RIO does not sample fast enough to create a root mean square (RMS) value and returns voltages equal to the portion of the wave at the time of measurement. The frequency of the controller is 18 kHz and the sampling rate of the RIO voltage bay is 15 samples per second which is close to 15 Hz. For this

reason, the current output using a shunt resistor varies greatly and is an unreliable measurement. Therefore a current transducer is used. The transducer is still not perfect at giving an RMS reading, even with the LabView interface, but it is much more accurate than the shunt resistor, which makes the extra cost worth it for this application.

4.3 Tachometer

Front and rear axle speeds are important in determining the torque input and output from the motors. Unfortunately, it is difficult to find a low-cost speed sensor which can readily interface with LabView. For this reason, an IES #330 Laser Photo Tachometer hand held digital speed sensor is used. The tachometer measures the rotational speed of the axles using a laser, therefore making it an unobtrusive measurement that will not directly affect the system. The sensor can accurately read the speed of the axle in revolutions per minute (RPM), which can manually be entered into the LabView program and then converted to rotational speed through the software. Since the motors on the front axle are all connected and the motors on the rear axle are connected, only one reading per axle is needed to determine the motor speeds for the entire system. This speed measurement system is thus limited to steady state measurements at this point in time as discussed later in Chapter 9 which is Future Research.

4.4 Accessories

The axles, belts and pulleys used for this system are the same parts that are used on small lawnmowers or tractors. These parts are readily available at relatively low cost. The axles are 3/8 inch diameter steel rods purchased from the hardware store, and the pulleys used are 3/8 inch bore, 2 inch diameter V slot die cast pulleys made by Chicago. The belts, which are found at any hardware store, are also V slot belts used on a small tractor or lawnmower. The pulleys used for the motors are the same Chicago die cast pulleys used for the axles, except they have a bore of 1/2 inch which is the diameter of the shaft on the motors. The diameter of the motor pulleys is still 2 inches so the motors and pulleys are all spinning at the same speed. The axle supports were ordered along with the frame from t-slots. They support screw into the frame and hold a 2 inch diameter bearing. The bearings were 2 inch diameter open face ball bearings from McMaster-Carr. The prices and ordering information for the accessories can be found in the Appendix in Table A-1.

5. HIL scaled down control strategy

The development of the control strategy for the HIL system is much like that of a real hybrid vehicle. There are two main propulsion plants, one on each axle, and various ways to distribute the load. For example, on a hybrid vehicle with a spark ignited engine and electric motor drive, it makes sense to assist the engine with the electric motor during acceleration because the engine in a hybrid vehicle is usually downsized and needs the added power. It then makes sense to load the engine with the BAS when the vehicle is cruising at constant speed to load the engine at a more efficient operating point and also to charge the battery pack for the electric drive. The HIL system can be used in the same way and tested in order to optimize the use of the engine and electric drive for the most efficient use of power during vehicle use. A comparison of the HIL architecture and the architecture of a “real” vehicle can be seen in Figures 12 and 13. The straight arrows, which represent road load are indicative of a force acting on the vehicle at the wheels. The circular arrows in the diagrams correspond to the sense of torque, not axle direction. The arrows are labeled with a negative or positive sign depicting the sense of the torque for the individual components. The axles and motor shafts always spin in the same direction. An example is when the BAS is loading the engine and recharging the high voltage battery for the rear traction motor. The front axle, engine shaft, and BAS shaft all spin in the same direction, but the BAS is applying torque in the opposite direction of the engine to load it and also create energy in the form of electrical power.

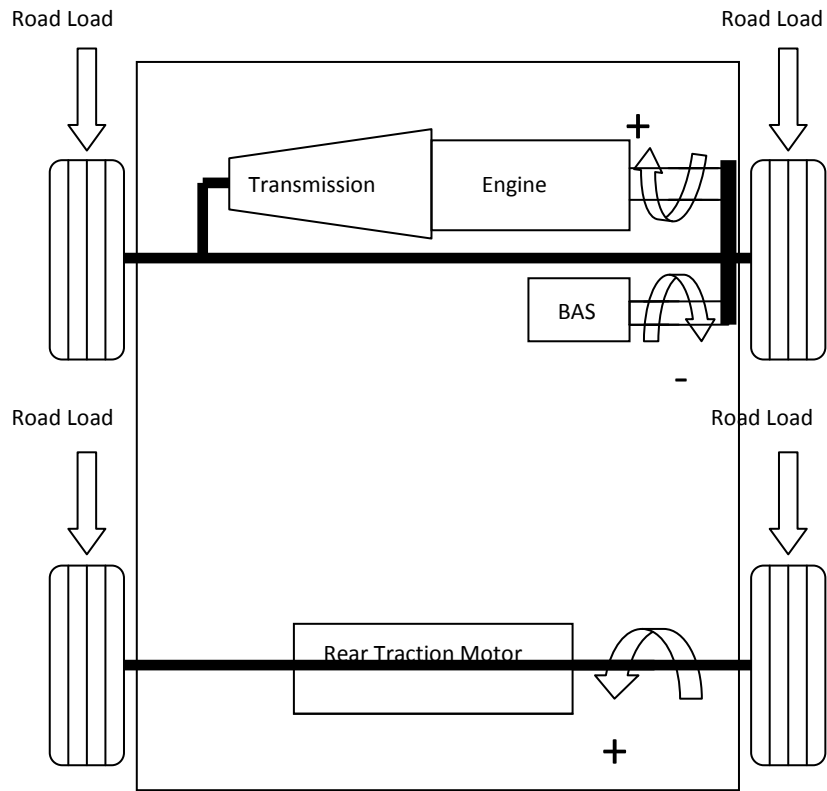


Figure 12. The powertrain and load component distribution of an actual hybrid vehicle.

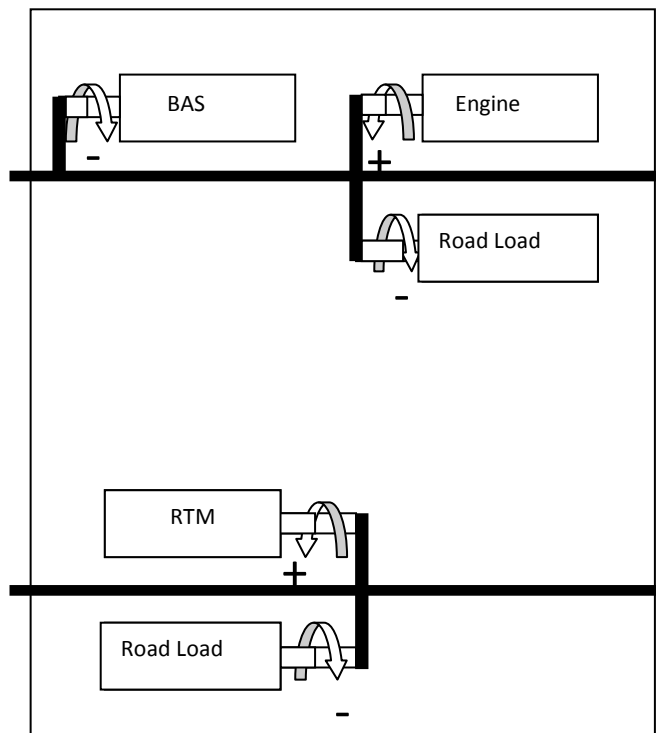


Figure 13. The HIL system configuration which simulates the powertrain components and various loads on a hybrid vehicle.

The front and rear axle of the system are not connected but can still be used in conjunction to measure the efficiency of the vehicle at different operating points. The resistors on the HIL system are variable resistance power resistors which can vary from 0-5 ohms. Since the resistance of the load can be varied, the “road load” on each axle can be varied as well as the load from the BAS which can be used to put extra load on the “engine” motor. The engine and rear traction motors on the HIL system can be individually controlled so the rear traction motor can be used when needed to assist the engine. Times when the assist could be useful are during times of large accelerations, short times of road grade, and short times of towing. The BAS resistance can then be used to load the engine motor which would then recharge the battery. Regenerative braking is also used to recharge the battery in most hybrid vehicles, and this can be done on the HIL model with the use of the proper motor controllers.

To develop an understanding for the control strategy of a HIL system for hybrid vehicles, an understanding of a few principles of automobile propulsion is necessary. The size and shape of vehicles is very important because of air resistance. The weight of a vehicle is also important. Aerodynamic drag force increases as the speed increases. The equation used to calculate aerodynamic drag, F_w , is

$$F_w = \frac{1}{2} \rho A_f C_D (V + V_w)^2 \quad (2)$$

where ρ is the air density, A_f is the frontal area of the vehicle, C_D is the aerodynamic drag coefficient which varies from vehicle to vehicle, V is the speed of the vehicle, and V_w is wind speed. Two other important force equations are that of inertia and tire rolling resistance, F_I and F_{RR} ,

$$F_I = ma \quad (3)$$

$$F_{RR} = N * C_{rr} \quad (4)$$

Where m and a are the mass and acceleration of the vehicle and N and C_{rr} are the normal force (mass times the acceleration of gravity, or mg) and tire rolling resistance coefficient. These equations show that as the velocity of a vehicle increases, so does the aerodynamic drag force acting on the vehicle, which is a key contributor to road load. The resistance that the powertrain of the vehicle experiences also comes from losses such as tire friction, gravity and vehicle weight. As the mass of the vehicle

increases, the forces required to accelerate the vehicle increase. The power of a vehicle is proportional to velocity times the force using the equation,

$$P_{aero} = FV \propto V^3 \quad (5)$$

Where P is power, F is force, and V is velocity. This relationship shows that the aerodynamic power of the vehicle is proportional to the V^3 . These equations show that the only force that varies quadratically with speed is the aerodynamic drag. The inertial force varies with acceleration while the rolling resistance varies with friction and normal load. The power dissipated from each of these forces does vary with speed due to the extra velocity term as in equation 5. Therefore, the inertial and rolling resistance powers are directly proportional to velocity. The load generators of the HIL system work in the same fashion as the aerodynamic drag of a vehicle. The higher the speed of the “driving” motor in the system, the larger the resistance or torque from each load generator due to the additional power input from the motor. As the load on the generators increase, so does the voltage drop created across the power resistors. The power load put on the generator motor can be calculated using Ohm’s Law,

$$P = VI \quad (6)$$

Where V is the voltage and I is the current through each generator. As a higher voltage is generated at a fixed resistance the current must increase to appease the system as shown,

$$R = \frac{V}{I} \quad (7)$$

This shows that as the voltage produced by the motor increases, so does the power generated from equation 6. For the case of increasing resistance (acceleration, grade, towing), as the resistance is increased, it will create a larger voltage drop across the resistor, which in turn creates a larger current flow. Equation 6 again shows that the power across the resistor will increase with a larger resistance which is consistent with additional forces on a vehicle. The shape of the speed versus power curves for both an actual vehicle and the HIL system shown in Figures 14 and 15 below indicate similar relationships between speed and power and help validate the HIL model as a substitute for the vehicle. The power determined for the vehicle in Figure 14 was calculated using the principles in Equations 2 and 5 and the assumption of a constant load, no

acceleration, a mass of 2000 kg, a C_D of .42 a frontal area of 2.69 m² and a C_{rr} of 0.007. These numbers were taken from the HEVT Equinox. The HIL model power chart was constructed using actual data which can be found in Table A-3. The power shown in Figure 15 is the electrical power dissipated through the resistors using Equation 6. The load on the motor was held constant during the test at 5 ohms.

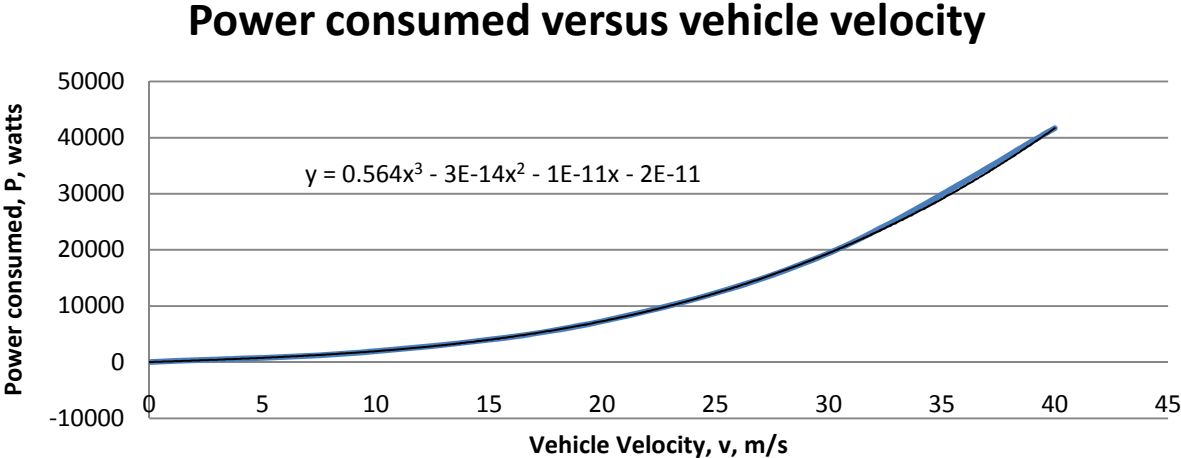


Figure 14. Relationship of velocity to power consumed by a vehicle.

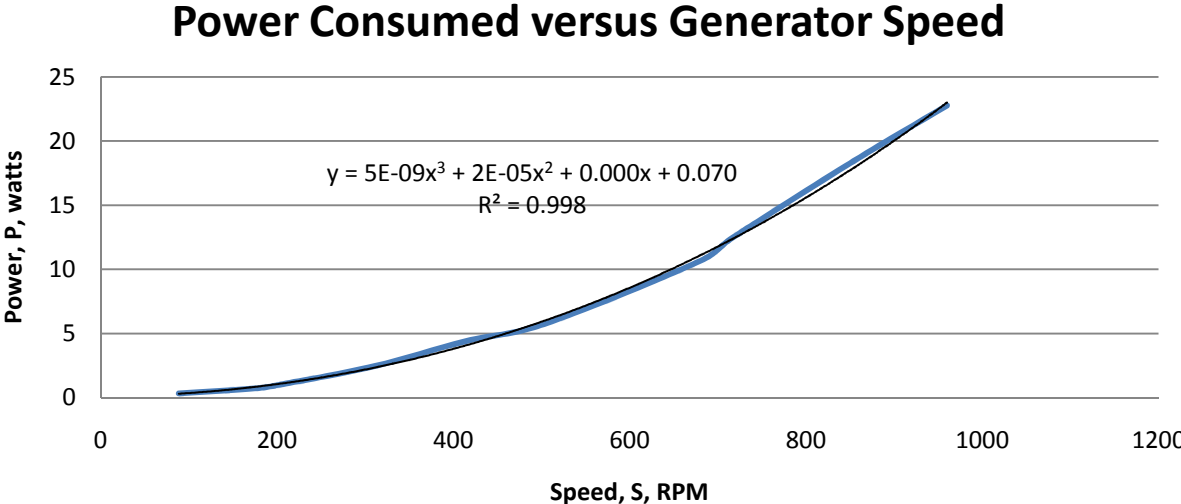


Figure 15. The relationship between motor speed and power of a generator for a fixed load resistance of 5 ohms.

The resistance of the loads can be adjusted from 0-5 Ohms, but the fundamental relationship between voltage and resistance still works like that of the aerodynamic drag force with speed. As the motors spin at higher speeds, the resistance or load on the motors increases therefore increasing the power consumed.

These principles can be used to explain the BAS on the vehicle also. As the speed of the engine increases on the vehicle, it spins the BAS, which is in regeneration mode, at higher speeds. The higher the generator spins, the larger voltage is produced by the generator. Since the terminal resistance of the generator is constant, the current must also increase therefore increasing the power at which the BAS can recharge the high voltage battery pack. If two-quadrant motor controllers were used that allowed the load motors to become generators much in the same manner as the BAS, this would allow for a better representation of engine loads as the engine speed changed along with regenerative energy capture of the vehicle.

6. Instrumentation

The measurements taken in the HIL system must all be compatible with the inputs and outputs of the CompactRIO. Figure 16 is a schematic of the system which looks complicated, but only because so many measurements are being taken from the system so it can be analyzed. As seen in the schematic, the RIO is outputting a 0-10 volt signal to the controllers, which is being used to simulate the voltage output by the potentiometers. The output has an update rate of 16 ksamples per second and resolution of 16 bits. The controllers use the voltage given by the RIO to produce a PWM signal which ranges from 0-24 volts to the motor when an input of 0-10 volts is given to the controller through the RIO. The controllers output at a frequency of 18 kHz. The remaining duties of the CompactRIO in this particular HIL system consist of reading the responses of the system into the LabView program for analyzation. The RIO is used to input and output signals. The voltage measurements are taken in parallel with the system components and should draw no significant current due to the high input impedance of the RIO. The measurements from 0-60 volts are sampled at 100 samples per second with 12 bit resolution, the 0-10 volt measurements are sampled at 500 ksamples per second with 12 bit resolution, and the millivolt measurements are sampled at 15 samples per second with 24 bit resolution. The current measurements are made both through shunt resistors and current transducers, and are read into the RIO as voltages. In the case of the shunt resistors, the RIO is given the data in millivolts, and for the current transducers, in volts. The connection between the 24 volt source for the battery is switched and fused so the system can be turned on and off and to protect the circuitry of the controllers if an abnormally large current is drawn from the batteries by the controllers. The power output by the driving motors is transmitted to the generator motors mechanically using a belt, pulley, axle system, much like one used on a car engine to power a belt driven accessory.

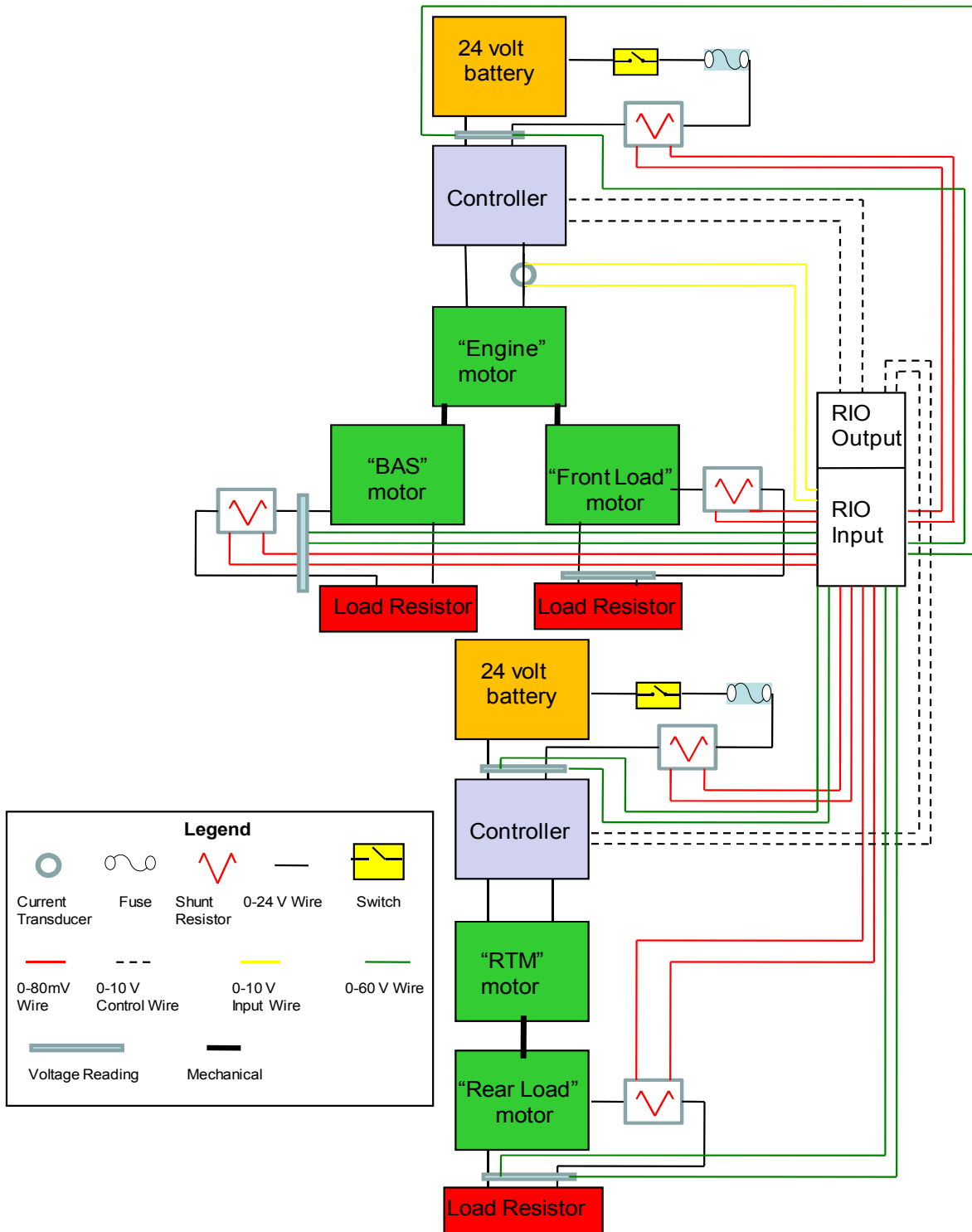


Figure 16. Schematic of the electrical and mechanical connections of the HIL system.

7. Test Procedure

This section describes how the parameters measured from the system by the Compact RIO are manipulated using LabView in order to create a model for the system. Certain assumptions and inferences must be made in order to analyze the HIL system without too much complexity. The model relies on a few basic fundamentals which will be explained below. The measurements and calculations for each component are also explained below. Certain component parameters and efficiencies are specified by the manufacturer.

The HIL system, just like an actual hybrid vehicle is designed to run at its most efficient state while still maintaining certain performance parameters. Items of interest in the system most generally have to do with power, torque, speed and efficiency. The power of a motor is output both as speed and torque. Motors generally run at high speeds and low torque loads or low speeds and high torque loads. The tradeoff is a design point which is heavily considered during vehicle development. The tradeoff has to do with gearing ratios. The vehicle can be designed to have high initial acceleration, which would therefore limit the top speed, or to have a higher top speed, but less acceleration. Since power, speed, and torque are all related to one another, generally speaking, if two of these variables are known, the third can be inferred. The system is designed and set up in such a manner that the power, speed and efficiency can be measured directly from the system using LabView, and the torque produced by the power plants and generated by the loads can therefore be inferred. The torque of the system is inferred instead of measured because it is much more difficult to accurately measure torque and read it into the RIO in a system like this than it is to measure voltage or current. The torque measuring devices are also very expensive to buy and implement in such a system.

7.1 Powertrain Motors

The powertrain motors drive the system and represent the spark ignited engine and rear traction motor. They are powered themselves by DC batteries and voltage controlled. The PWM voltage from the controller into the motors, V_{supply} , can be found using the equation

$$V_{supply}(V) = dV_{PT} + \frac{E*s}{1000} \quad (8)$$

Where dV is equivalent voltage explained below and E is the back EMF of the motor which is 11.5 V/kRPM . The speed of the motor, s , which is in RPM is divided by 1000 due to the units of the back EMF constant. The voltage drop across the motor, dV_{PT} , is calculated using the equation

$$dV_{PT}(V) = I_{controller} * R_{motor} \quad (9)$$

Where $I_{controller}$ is the PWM current output by the controller and R_{motor} is the motor resistance found across the terminals as seen in Figure 17.

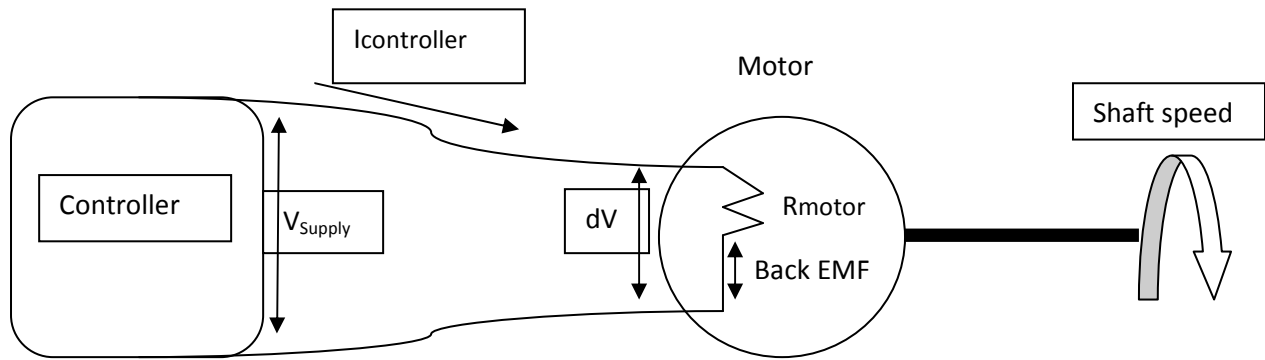


Figure 17. Diagram for calculation of dV_{PT} in equation 7.

Since the motor and controller are connected to each other in series, the voltage drop across the components can vary, but the current should be the same through the loop. With the current remaining constant, the power output by the motor, $P_{out,PT}$, is calculated using the equation

$$P_{out,PT} (W) = dV_{PT} * I \quad (10)$$

The power input $P_{in,PT}$ to the motor is found in a similar fashion to the power output, but taking into account the back EMF loss in the motor using the equation

$$P_{in,PT} (W) = V_{supply} * I \quad (11)$$

A second way to calculate the power output which includes mechanical losses in the motor uses the equation for initial rotor torque. The torque of the power developing motors can be calculated a few different ways. For model accuracy and simplicity, the torque constant, t_c , which is given by the manufacturer is in the equation

$$T_{PTi} (Nm) = I * t_c \quad (12)$$

Where in this case t_c is equal to 0.11 Nm/amp. Next factoring in the torque loss due to windage and bearing loss of the motors, T_f , which can be considered constant, the shaft torque output of the motors, T_{PTo} , is found using the equation

$$T_{PTo} (Nm) = T_{PTi} - T_f \quad (13)$$

The value specified by the manufacturer for windage and bearing torque loss of these particular motors is 0.12 Nm. The power output using the torque method can then be calculated using the equation

$$P_{out,PT2} = T_{PTo} * S \quad (14)$$

Where S is the speed of the shaft. The efficiency of the motors can be calculated using the equation

$$\eta_{m,PT} = \frac{P_{out,PT}}{P_{in,PT}} \quad (15)$$

Basically, the efficiency or difference in power input to output is the voltage drop across the motor terminals plus the back EMF created in the motor due to the windings.

7.2 Load Motors

The load motors used as generators are connected to the powertrain motors mechanically which makes it difficult to directly find the input power without a direct torque measurement. In the model, the torque input and power input are found indirectly using motor constants. The power output across each power resistor, $P_{LM,o}$, is found using

$$P_{LM,o} (W) = VI \quad (16)$$

where V and I are the voltage and current flowing across the power resistor. As seen in Figure 16, each generator spins at a varying speed which produces a corresponding voltage. Since the resistance is constant at this point, the current must also increase resulting in the power output, $P_{LM,o}$. To find the power input, the torque of the load motor, $T_{LM,i}$, is found using the torque constant and friction torque as it was for the powertrain motors resulting in the equation

$$T_{LM,i} (Nm) = I * t_c + t_f \quad (17)$$

The assumption that the current does not change through the series connected system still holds true for this case. The power input to the system can be inferred using the load motor torque and the speed of each axle. Since the axle speed, s , is measured in RPM, it must be converted to angular velocity, ω , using the conversion factor

$$\omega \left(\frac{r}{s} \right) = \frac{2\pi}{60} * s \quad (18)$$

Once the speed has been converted to radians per second, the input power to the load motors, $P_{LM,i}$, is found using the equation

$$P_{LM,i} (W) = T_{LM,i} * \omega \quad (19)$$

Where ω will vary as the speed of the driving motor and is determined by the controller voltage output. The axle speed can also be different for the front and rear axles because they are not connected. The speed is input into the model using a hand held digital tachometer. Now since the input and output power of the load motors has been determined, the efficiency of the motors as generators, η_{LM} , can be found from

$$\eta_{LM} = \frac{P_{LM,o}}{P_{LM,i}} \quad (20)$$

There are other ways to measure the efficiency of the load motors including attempting to calculate the voltage drop across the motor, but the current and speed measurements are direct measurements which are accurate and reliable. Also, since torque is a parameter of interest, it needs to be calculated anyways. A sample calculation of actual test data can be found in the Appendix.

7.3 Controllers

For many cases both in conventional and hybrid vehicles, component efficiency which is calculated reports both the efficiency of the component and its controller. In this case, the efficiencies given are only the actual efficiencies of the motors. The power into the controller from the batteries, $P_{cont,i}$, can be directly measured with the RIO

$$P_{cont,i} (W) = V_{cont,i} * I_{cont,i} \quad (21)$$

Where $V_{cont,i}$ and $I_{cont,i}$ are the voltage and current fed to the controller from the batteries. The batteries at a high state of charge produce 24 volts to the controller. As the controller demands current from the batteries, the voltage sags slightly. The output of the controllers when connected to the motors has many dependencies including motor speed and load. To ensure a steady controller power output, $P_{out, resis}$, one of the

controllers was then placed in series with a power resistor and thus no motor. The efficiency of the controller was then found using

$$\eta_{cont} = \frac{P_{out,resis}}{P_{cont,i}} \quad (22)$$

Controller efficiency is largely a function of both I and I^2 . Therefore a map of controller efficiency was easily found and incorporated into the model as seen in Figure 18. The data can be seen in Table A-2 in the Appendix.

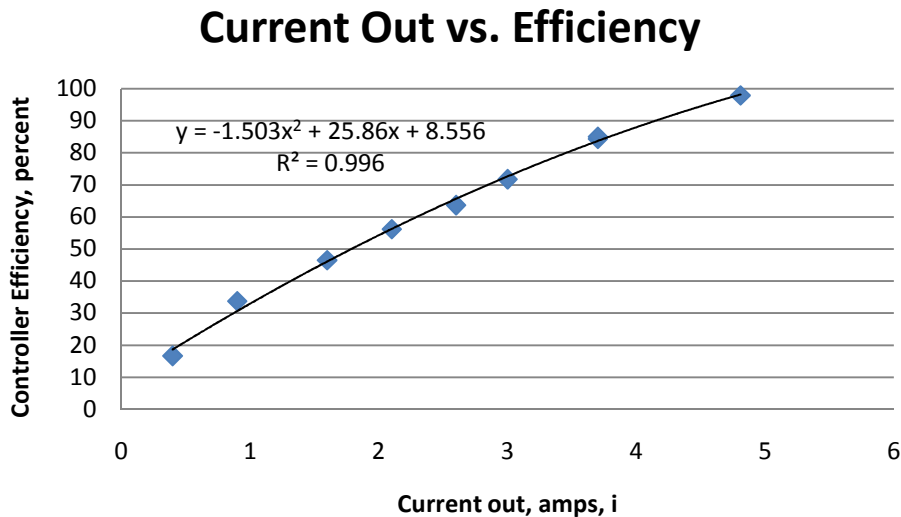


Figure 18. Efficiency map of the Dart controllers as a function of I^2 .

The map shows that the efficiency of the controller increases as the output current of the controller increases. The controllers, which are designed to control DC permanent magnet motors would not output a current draw higher than 4.81 amps to the power resistors even as the resistance was varied. The reason for the controller current being limited to 4.81 amps is with a 24 volt source and a 5 ohm resistance, that was the maximum current that could be drawn without increasing the input voltage. For this reason, the curve needed to be extrapolated past that current draw for the actual HIL system. The efficiency of the controller at 4.81 amps was 97.9%. Since there have to be losses in the controller even at higher currents than 4.81 amps, the map was cut off at 4.81 amps and the controller efficiency is capped at 97.9% in the model for currents greater than 4.81 amps.

7.4 Mechanical Losses

There are numerous mechanical losses in the system that are too difficult to measure and calculate in real time, so they are measured in steady state. The powertrain motors and load motors in the HIL system are connected mechanically through an axle supported by bearings. The motor shafts are connected to pulleys which couple with pulleys on the axle and are joined by belts. Losses in this system can include bearing losses, belt friction and belt slip and axle distortion. These losses can become quite significant in a poorly designed system and occur not only in the HIL system, but also in vehicle systems on belt-driven components such as air conditioning compressors and alternators. Tests were conducted to measure the significance of the mechanical loads on the system. These tests do not directly correlate to the HIL system as it currently runs, but they do indicate that the mechanical losses in the system are significant. The tests run determine the power absorbed to spin a motor at the same speed under different mechanical loading situations and the results are shown in Table 3.

Table 3. Tests were run to help understand the magnitude of HIL system mechanical losses				
Load	Speed (RPM)	V (volts)	I (amps)	P (Watts)
motor unloaded	1080	23.79	0.43	10.23
motor spinning axle, bearings, pulley and belt	1080	23.58	0.99	23.27
motor spinning a second unloaded motor using an axle, bearings, pulley and belt (Road Load)	1080	23.38	1.95	45.52
motor spinning unloaded motors using an axle, bearings, pulley and belt (BAS and Road Load)	1080	23.23	3.43	79.68

While it is hard to quantify specific component efficiencies of the axle-pulley system, it is obvious that losses do exist. As seen in the table, when multiple mechanical components are added to the system, losses can become quite significant. The losses shown above are only for the front axle when the load motors are not loaded or connected to power resistors.

7.5 Overall Axle

Component efficiency is very important in hybrid vehicles, which is why each component is monitored. However the main goal in hybridizing a vehicle is to achieve maximum efficiency of the overall system. The HIL model does this for each axle, which can, in turn be used to find overall efficiency. The calculation for overall axle efficiency is an easy one, but very important. It includes all losses in the system, inclusive of but not limited to battery to controller losses, internal controller losses, controller to motor losses, internal motor losses, mechanical coupling losses (bearing and belt), generator losses, and losses in the power resistors (vehicle propulsion load). The efficiency of each axle, η_{axle} , is

$$\eta_{axle} = \frac{\Sigma((V * I)_{resistor})}{(V * I)_{battery}} = \frac{\Sigma(P_{resistor})}{P_{battery}} \quad (23)$$

Where $P_{resistor}$ is the sum of the power drawn from each power resistor on the axle and $P_{battery}$ is the amount of power drawn from the source or battery of the model. Each of these is a direct measurement taken from the RIO. This is a very repeatable and accurate calculation.

7.6 Limitations

7.6.1 Use of DC motors

The HIL system can be used to model a hybrid vehicle fairly accurately. There are however, a few limitations to the system. One of the limitations is that the motors on the HIL system are all permanent magnet motors which can be mapped to model other types of powertrain components such as fuel cells or spark ignited engines, but they do not behave exactly the same as these alternate types of powertrain components.

7.6.2 Regeneration energy capture

A second limitation is that when the system acts in regeneration mode, the regeneration can be calculated using LabView, but does not actually take place. The DC controllers do not possess the ability to regenerate the DC batteries used in the system. The system can still be used to determine the efficiency of the vehicle in different modes, but the actual amount of energy which can be regenerated to the high voltage system or battery pack of a hybrid vehicle cannot be accurately modeled. Two types of regeneration that are commonly used in hybrid vehicles are a high voltage alternator (BAS) which is belted to an engine, or regenerative braking. The regeneration efficiency of these components is not 100%, but their regeneration efficiency can be approximated. It is possible to use regeneration enabled controllers, but they are difficult to find and more expensive than the Dart controllers currently running on the system. The controllers needed to capture energy generated by the motors are 2-quadrant controllers (plus and minus torque) which means they can drive a motor and capture energy from a generator, but cannot spin the motors in reverse direction without changing the polarity of the motor leads.

7.6.3 Speed sensing

A third limitation has to do with the axle speeds on the system. The axle speed is currently measured using a hand-held digital tachometer. The speeds are then input to the LabView program by hand. This limits the dynamic response measurement of the system. The efficiencies cannot be compared with changing axle speed unless the hand measurements are taken and entered into the program. Speed sensors which are self powered and compatible with the input of a RIO need to be found and implemented into the system to overcome this limitation.

8. Test Results

A separate LabView code was created to test and verify the HIL system. The code was identical to the original program with the exception of the controller output portion. In the original code, the controller output is controlled by the user using the LabView interface while both the program and the HIL system are running. The test code, which will be useful for displaying the system, introduces the ability to predetermine and enter a drive cycle to the system. This allows the system to run with no user interaction. Currently, since there is no dynamic measurement of the axle speeds of the system, the efficiency and torque calculations will not be exactly correct. The drive cycle mode does, however, prove the usefulness potential of the system.

8.1 Drive Cycle Creation

The drive cycles for the HIL system are constructed by hand in the LabView code. The difference from the normal code used for the system is the powertrain control input. The normal code consists of a place on the interface for the user to enter the controller output level on a scale of 1-10. The drive cycle uses a timed for-loop and user controlled sized array to pre-enter a drive cycle as seen in Figure 19. The for-loop has a timer which in this instance is set to take a new value from the array every 3 seconds. The values given to the controller are constants stored outside of the for-loop in an array. The for-loop reads the values in order from top to bottom of the array. The engine input box in the Figure 19 is the same input used on the original code, but it reads in the array values rather than a user input. The cycles are easily designed and changed with this method programming. To create a different drive cycle, the only changes necessary are new values in the array and possibly a different timer value that the for-loop uses to read in the values of the array.

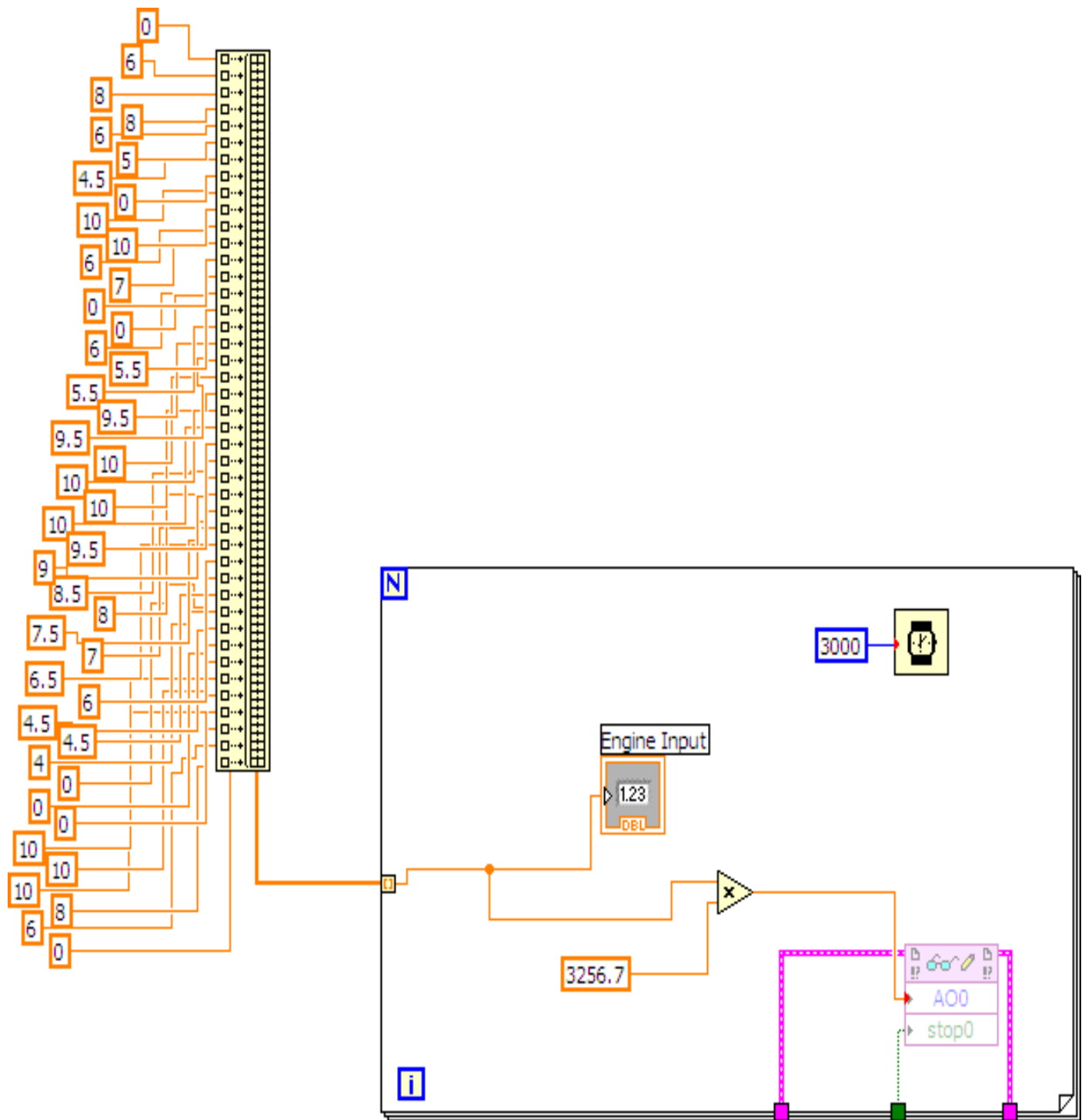


Figure 19. Example of the programming code used to create a predetermined drive cycle in LabView

8.2 Simple Drive Cycle

To test both the drive cycle program, and the HIL system, the first drive cycle constructed was very simple. The array instructed the HIL system to start from rest, accelerate as quickly as possible to full speed, run at full speed for a given amount of time, and decelerate back to rest as seen in Figure 20.

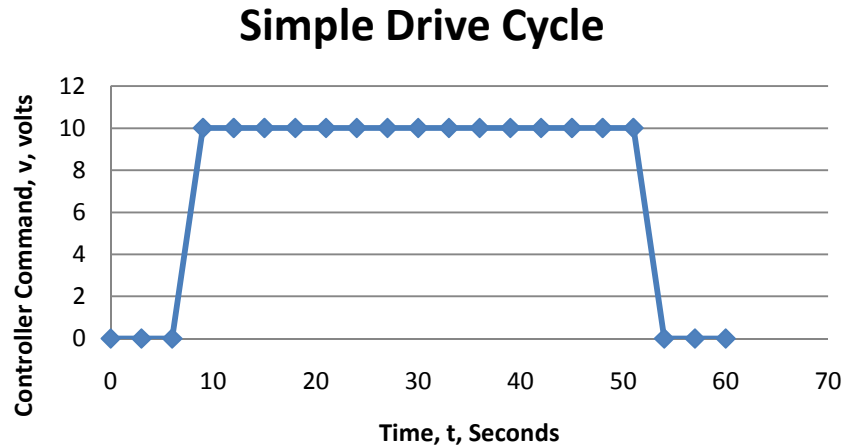


Figure 20. Simple drive cycle used to test and validate the HIL system.

The other purpose of the simple drive cycle was to show the ability of the system to simulate a vehicle if a dynamic speed sensor were available. This simple drive cycle allowed the user enough time to measure the axle speed with the hand tachometer and enter it into the interface. The efficiencies of the powertrain motors, generators, and axle were all then calculated along with the torques from the motors as seen in Figure 21.

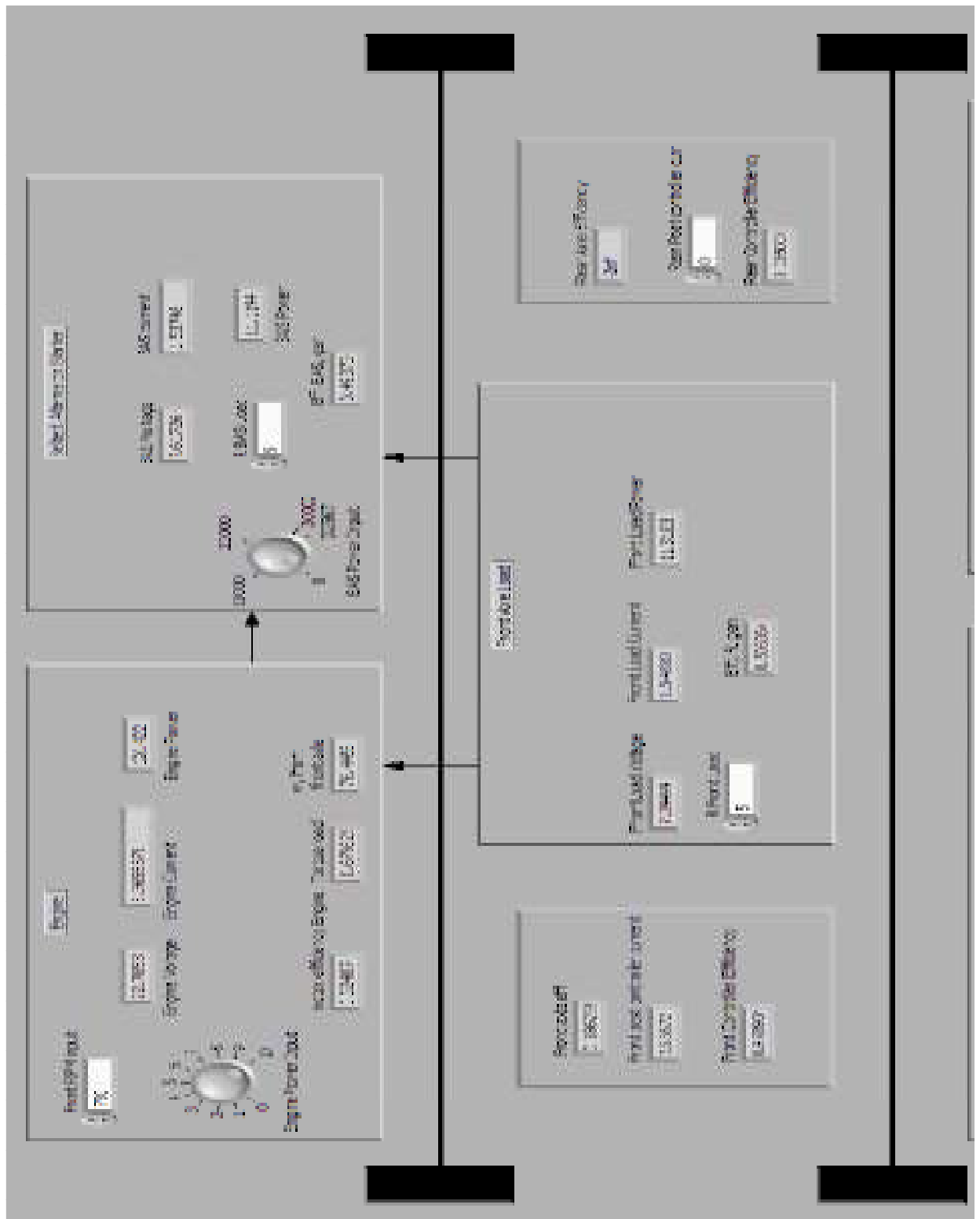


Figure 21. Power and efficiency outputs during the simple drive cycle at full speed.

As seen in the Figure 20, the input to the controller is 10 volts, which is the highest possible output from the controller. The engine is running at 32% efficiency while the BAS and Axle load are running at 49% and 51% efficiency respectively. The overall axle efficiency is 18.6%. Sample calculations for the results in Figure 21 can be seen in the Appendix. Keep in mind that the numbers are not identical because the system is constantly varying slightly due to the PWM controller reading. Some of the efficiencies had not refreshed on the screen before the print screen button was applied.

The resistances and axle speed were put manually into the program while it was executing. For this reason, before a computer read speed measurement is implemented into the system, the only data taken can be for constant axle speed. For this case the resistor for both the BAS and front axle load are set to 5 ohms, which means they are both applying the same amount of load to the engine. In most cases, the BAS load will not be as significant as the road load (which is part of the control strategy), but this test was run to verify the system and drive cycle program work properly. As seen from Figure 21 and the sample calculations, the speed was set at 730 RPM, the front engine efficiency was 33.8%, the BAS efficiency was 53.0%, the axle load generator efficiency was 51.2% and the overall efficiency of the front axle was 24.0%.

8.3 Complex Drive Cycle

Since the speed measurement is not dynamic, it is hard to characterize a complex drive cycle. Constructing and running a complex cycle reiterates the point that a RIO compatible dynamic speed sensor would be very useful in the HIL system. The complex drive cycle is useful for display purposes however. An arbitrary middle of the road axle speed can be entered into the system. Using this axle speed the entire cycle, the concept of simulated a vehicle drive cycle can still be understood. An example of a complex drive cycle developed in LabView is shown in Figure 22.

Complex Drive Cycle

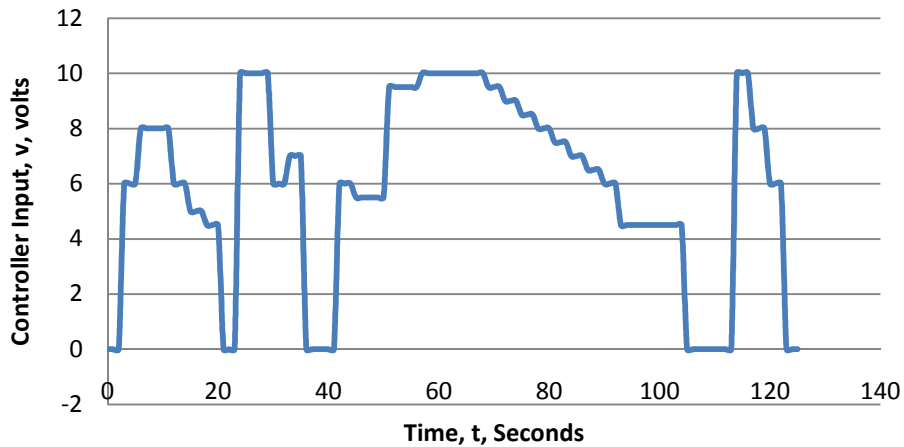


Figure 22. Example of a more complex drive cycle that can be simulated using the HIL system.

The complex drive cycle is very dynamic. There are moments of large acceleration and deceleration along with some constant speed inputs. This drive cycle is much more typical of an actual vehicle than the simple drive cycle shown before. Even though this is more indicative of a city drive cycle with stop lights and traffic, true highway drive cycles are very dynamic also for the most part. A cycle like the simple one shown before virtually never happens in real life, therefore it is important for the HIL system to be able to simulate actual drive cycles like the one shown in Figure 22.

9. Future Research

The main purpose of this research was to design and build a HIL system which can be used to develop and test a control strategy for the REV_{LSE} Equinox hybrid vehicle built by the Hybrid Electric Vehicle Team. The HIL system is also designed with the flexibility of simulating other hybrid architectures. The system works and calculates efficiencies of the system. A key point in the development of the LabView program included making the program user-friendly. The program should be self-explanatory and logical to use. The future work with the system includes using the system to develop a control strategy for year four of the Challenge X competition. Different drive cycles can be developed in LabView in order to test various control strategies for comparison. The use of the various hybrid components can be optimized for maximum vehicle efficiency.

There are improvements which could be implemented to the system in the future if funding and time allow. If two-quadrant controllers can be found at an affordable price that would allow actual regeneration from the BAS load and regenerative braking from the axles back into the battery, the system will become a more accurate model. These controllers would add complexity to the code and add a considerable time and money cost to the project. The controllers used to control the powertrain motors can still be used in the model. The system can currently use the power drawn by the power resistors and known regeneration efficiencies from the vehicle to predict the regeneration of the system, but this is not as accurate of a model as using regenerative controllers.

A second potential future improvement involves the axle speeds of the system. Currently the speeds are measured using a digital hand held tachometer. The speeds are then entered into the LabView program manually. This method of measurement was chosen due to the cost of speed measurements which would be compatible with the 4 bay Compact RIO and available modules. The sensors would need to report the speed of the axles as a voltage to the RIO which could be converted into a speed using the LabView program. Another type of speed measurement output, such as frequency, would require an additional module and bay in the RIO module. Use of these sensors would allow for dynamic measurements during axle speed changes. The system currently will only measure efficiencies for a given axle speed.

The major aspect of the future research on this HIL system will be using the system to input drive cycles and using it to analyze the performance of the hybrid architecture. The purpose of the system is to simulate and test the control strategy of

the Equinox built by the HEVT. The Equinox, which has the SPA simulated by the current HIL system setup, has two separate powertrain components which are run individually. Therefore, the control strategy of the vehicle determines which components are powering and/or loading the system at any given time to find the most efficient strategy to run the vehicle. The models for each of the components on the actual vehicle need to become part of the efficiency model in the HIL system. Each component on the vehicle has an efficiency map of the loading and speed versus the efficiency of the component. It will be nearly impossible to incorporate the actual maps into the HIL system since some of the PM motors are less efficient than the vehicle components, but the difference in component efficiency should play a role somehow in the model. For example, the RTM which is an electric drive runs much more efficiently than an internal combustion engine. Currently on the model, they run at basically the same efficiency. Once models for the efficiency of each component during various loading schemes are complete, the HIL system will be very accurate in determining overall system efficiency. The HIL system can run different drive cycles with different components of the system powering and loading the system. Through similar testing, the most efficient control strategy for the vehicle can be found without ever needing the actual vehicle on hand. This is very convenient for the other sub-teams since they will also need the vehicle running for testing.

10. Conclusion

This paper discusses a scaled down model hardware-in-the-loop hybrid (HIL) control system. It explains the need and usefulness of using HIL systems during the development and validation of vehicle components and control strategies. The configuration of the system constructed is variable, but the setup is the split parallel architecture (SPA) which is the configuration of the vehicle under development by the Hybrid Electric Vehicle Team (HEVT) of Virginia Tech. Brushed permanent magnet DC motors are used in place of a spark ignited engine, belted alternator starter, and rear traction motor. The motors are controlled by a computer interface. This paper explains the considerations and selections of all of the components of the HIL system, including using National Instruments' Compact RIO and LabView as the computer interface. The test procedure was introduced in great detail including the equations and calculations performed by LabView. The actual setup and schematic of electrical connections of the system are shown and discussed.

This paper also presents the implementation of computer controlled drive cycles to help validate the system. Even though a few component additions could strengthen the performance of the system, the drive cycles and results prove the usefulness of the HIL system as a model for designing control strategies for hybrid vehicles. The system runs by itself and outputs component and overall efficiencies as well as motor torques. These outputs are vital in determining a control strategy. The best control strategy is one that allows the system to run continuously with the highest possible overall tank to wheels efficiency. The system allows this design process to be completed without using the actual vehicle as a test stand.

The research objectives set in the introduction were all met while building the HIL system model. The model represents the powertrain configuration of the HEVT REV_{LSE}. Regenerative controllers would provide a more accurate model of the vehicle, and can be implemented during future work. The model has proven useful for determining system efficiencies during different drive cycles and can do the same for different component use and can also analyze the data input to the RIO using LabView. The system can now be used in the future to develop and validate a control scheme for an actual vehicle so the vehicle will be available to other teams for on road testing.

References

1. Boyd, Steven J. (2006), "Hybrid Electric Vehicle Control Strategy Based on Power Loss Calculations" MS Thesis, VPI&SU, Blacksburg, Va..
2. Guhmann, Winkler, "Hardware-in-the-Loop simulation of a hybrid electric vehicle using Modelica/Dymola," Germany, Technical University of Berlin, 2007.
3. Dynasim, "Hardware-In-the-Loop Simulation of Physically Based Automotive Models with Dymola (Application Note)," Sweden, Lund, July 11, 2003.
4. Abourida, Dufour, Belanger, "Real-Time and Hardware-In-The-Loop Simulation of Electric Drives and Power Electronics: Process, problems and solutions," International Power Electronics Conference, 2005 April 4-8 Niigata, Japan pgs 1908-1913.
5. Lohse-Busch, H., T. Stinchfield, M. Mital, A. Hines, and D.J. Nelson (2004), "Design And Implementation Of A Hybrid Electric Vehicle Powered By A Hydrogen Engine" SAE Paper 2004-01-0194, 2004 SAE Congress, 3/8 - 3/11, Detroit, Mi., 18 pages.
6. Boyd, Steven, Paul Hiester, Seth Lawson, Dustin Sheffield and Douglas J. Nelson (2006), "Design and Development Process for the Equinox REVlse E85 Hybrid Electric Vehicle", 2006 SAE International World Congress, 4/3 - 4/7, Detroit, Mi., paper 2006-01-0514, 19 pgs.

Appendix

C34 SERIES SPECIFICATIONS – *Continuous Stall Torque 63 - 125 oz-in (0.445 - 0.883 Nm)* *Peak Torque 580 - 1110 oz-in (4.096 - 7.838 Nm)*

Part Number*	C34-L60				C34-L70				C34-L80				
	10	20	30	40	10	20	30	40	10	20	30	40	
Winding Code**													
L = Length	inches	6.00				7.00				8.00			
	millimeters	152.40				177.80				203.20			
Peak Torque	oz-in	580.0	580.0	580.0	580.0	855.0	855.0	855.0	855.0	1110.0	1110.0	1110.0	1110.0
	Nm	4.096	4.096	4.096	4.096	6.038	6.038	6.038	6.038	7.838	7.838	7.838	7.838
Continuous Stall Torque	oz-in	63.0	63.0	63.0	63.0	95.0	95.0	95.0	95.0	125.0	125.0	125.0	125.0
	Nm	0.445	0.445	0.445	0.445	0.671	0.671	0.671	0.671	0.883	0.883	0.883	0.883
Rated Terminal Voltage	volt DC	12 - 30	12 - 48	18 - 60	30 - 72	12 - 30	12 - 48	18 - 78	30 - 120	12 - 30	12 - 48	18 - 90	30 - 132
Terminal Voltage	volt DC	24	36	60	72	24	36	48	72	12	24	48	72
Rated Speed	RPM	2700	1800	1447	952	4450	2720	1800	1313	1800	1750	1847	1424
	rad/sec	282.74	188.97	151.53	99.69	468.00	284.84	188.50	137.50	188.50	183.26	193.42	149.12
Rated Torque	oz-in	60.7	55.1	63.8	76.1	75.0	110.0	85.0	86.1	81.7	84.9	80.4	110.0
	Nm	0.43	0.39	0.45	0.54	0.53	0.78	0.60	0.60	0.58	0.67	0.57	0.81
Rated Current	Amps	8.20	3.70	2.05	1.55	13.00	7.00	3.75	2.15	15.00	8.50	3.70	2.50
Rated Power	Watts	121.3	77.5	60.4	53.6	247.0	221.4	113.2	80.4	106.6	122.9	108.9	121.2
	Horsepower	0.16	0.10	0.09	0.07	0.33	0.30	0.15	0.13	0.15	0.16	0.15	0.16
Torque Sensitivity	oz-in/amp	10.80	21.80	43.60	68.00	7.79	15.56	31.20	59.00	7.50	15.00	30.00	60.00
	Nm/amp	0.08	0.15	0.31	0.48	0.06	0.11	0.22	0.42	0.05	0.11	0.21	0.42
Back EMF	volt/KRPM	8.00	16.10	32.20	90.30	5.76	11.50	23.00	43.60	5.50	11.00	22.00	44.40
	volt/1000rad/sec	0.08	0.15	0.31	0.48	0.06	0.11	0.22	0.42	0.05	0.11	0.21	0.42
Terminal Resistance	ohms	0.43	1.72	6.80	14.50	0.14	0.56	2.24	7.40	0.15	0.60	2.40	4.90
Terminal Inductance	mH	0.90	4.80	18.00	35.00	0.24	1.12	4.50	14.50	0.18	0.72	3.10	11.20
Motor Constant	oz-in/watt ^{1/2}	16.62	16.62	16.72	17.86	20.82	20.82	20.85	21.69	19.36	19.36	19.36	27.11
	Nm/watt	0.12	0.12	0.12	0.13	0.15	0.15	0.15	0.15	0.14	0.14	0.14	0.19
Rotor Inertia	oz-in-sec ²	0.030	0.030	0.030	0.030	0.042	0.042	0.042	0.042	0.055	0.055	0.055	0.055
	g-cm ²	2118.45	2118.45	2118.45	2118.45	2965.83	2965.83	2965.83	2965.83	3893.83	3893.83	3893.83	3893.83
Friction Torque	oz-in	15	15	15	15	17	17	17	17	20	20	20	20
	Nm	0.11	0.11	0.11	0.11	0.12	0.12	0.12	0.12	0.14	0.14	0.14	0.14
Thermal Resistance	°C/watt	3.90	3.90	3.90	3.90	3.70	3.70	3.70	3.70	3.50	3.50	3.50	3.50
Damping Factor	oz-in/KRPM	2.50	2.50	2.50	2.50	3.00	3.00	3.00	3.00	3.80	3.80	3.80	3.80
	Nm/KRPM	0.02	0.02	0.02	0.02	0.02	0.02	0.02	0.02	0.03	0.03	0.03	0.03
Weight	oz	100.00	100.00	100.00	100.00	128.00	128.00	128.00	128.00	152.00	152.00	152.00	152.00
	g	2834.95	2834.95	2834.95	2834.95	3628.74	3628.74	3628.74	3628.74	4309.12	4309.12	4309.12	4309.12
Electrical Time Constant	millisecond	2.0930	2.7907	2.6471	2.4138	1.7143	2.0000	2.0089	1.9595	1.2000	1.2000	1.2917	2.2857
Mech. Time Constant	millisecond	15.4888	15.39267	15.21369	13.31555	13.72031	13.74418	13.72856	12.64995	20.94	20.94	20.94	10.99184
Speed/Torque Gradient	rpm/oz-in	-4.931193	-4.900564	-4.843981	-4.23927	-3.120097	-3.125523	-3.121516	-2.876691	-3.636364	-3.636364	-3.636364	-1.839339

Figure A-1. Complete specifications list for Moog C34 L70-20 motors.

SPECIFICATIONS

	65E10
Load current (continuous)	10 amps
Speed adjustment	5K Ω potentiometer or 0 to +10VDC input signal
Speed range	30 : 1
Overload capacity	200% for 10 seconds; 150% for one minute
Current limit	adjustable 100% to 200% of full motor load, up to 200% of control current rating
Acceleration	adjustable - 0 to 10 seconds
Deceleration	non-adjustable - 0.5 seconds
Maximum speed	adjustable - 50 to 100% of base speed
Minimum speed	adjustable - 0 to 30% of max speed
Connections	Euro-style terminal block (14Ga. to 28Ga.)
Speed regulation	1% of base speed via adjustable I.R. Compensation trimpot
Operating temperature	-10°C to +45°C (14°F to 113°F)
Package configuration	black anodized aluminum extrusion
Internal operating frequency	approximately 18K Hertz

Figure A-2. Complete specifications for Dart 65E10 controller.

Table A-1. Cost and contact/ordering info for parts.

Component	Source	Cost
Motors (C34L70-20)	Moog Inc- Wanda Wilson (828-837-5115)	\$176 each
Controllers (65 E 10)	Dart Motors- Danny Arnell (804-727-4200)	\$144.04 each
Power Resistors	Digikey D225k5R0E	\$27.76 each
Frame	Futura Industries- Allen Perry (800-824-5753)	
	2 peg corner (653047)	\$2.76 each
	4 peg corner (653073)	\$5.67 each
	2 peg strip (653046)	\$3.39 each
	bearing holder (659044)	\$31.75 each
	Double T nuts (651490)	\$0.89 each
	TS 10-10	\$0.23 per inch
	cut of 10-10	\$1.85 per cut
Bearing	McMaster-Carr 6383K23	\$3.88 each
Shunt Resistors	CSA100-100 www.rc-electronics-usa.com/current-shunt.html	\$21.95 each
RIO Modules	NI (888-280-7645)	\$300-400 each
belts, pulleys	Tractor Supply Company (540-381-7630)	\$3-8 each
Current Transducers	H970-LC-B Flex Core- Steve- 614-889-6152	\$240 each
Total Spent		\$3135.03

Table A-2. Data collected from controller efficiency tests.

Controller Characteristics Using a load of a 5 ohm 225 watt power resistor									
Voltage in (V)	24.2	24.7	24.5	24.3	24.2	24.7	24.3	24.1	24.3
Current In(amps)	3.3	0.2	1.1	2.2	3.3	0.5	1.6	4.85	2.6
Voltage Out (V)	18.2	2.05	7.84	13.08	18.34	4.63	10.41	23.8	15.1
Current Out (amps)	3.7	0.4	1.6	2.6	3.7	0.9	2.1	4.81	3
Power In (W)	79.86	4.94	26.95	53.46	79.86	12.35	38.88	116.8	63.2
Power Out(W)	67.3	0.82	12.5	34.0	67.8	4.16	21.8	114.4	45.3
Efficiency	0.843	0.165	0.465	0.636	0.849	0.337	0.562	0.979	0.716
Current Out^2	13.69	0.16	2.56	6.76	13.69	0.81	4.41	23.11	9

Table A-3. Speed versus power measurements for Motors			
Speed (RPM)	Voltage (Volts)	Power (watts)	
88.4	1.29	0.332	
175	1.9	0.722	
210	2.35	1.10	
310	3.5	2.45	
413.7	4.69	4.39	
507	5.4	5.83	
680	7.3	10.6	
717	7.9	12.4	
854	9.6	18.4	
960	10.67	22.76	

Sample Calculations and Results from a Constant Axle Speed Drive Cycle from Figure 21.

Front Engine:

$$dV_{PT} = I_{controller} * R_{motor}$$

$$dV_{PT} = 7.64\text{amps} * .56\text{ohms} = 4.28 \text{ volts}$$

$$V_{supply}(V) = dV_{PT} + \frac{E * S}{1000}$$

$$V_{supply}(V) = 4.28 \text{volts} + \frac{11.5V \cdot 730RPM}{1000 \cdot kRPM} = 12.68 \text{volts}$$

$$P_{out,PT} (W) = dV_{PT} * I$$

$$P_{out,PT} (W) = 4.28 \text{ volts} * 7.64 \text{ amps} = 32.70 \text{ watts}$$

$$P_{in,PT} (W) = V_{supply} * I$$

$$P_{in,PT} (W) = 12.68 \text{ volts} * 7.64 \text{ amps} = 95.87 \text{ watts}$$

$$\eta_{m,PT} = \frac{P_{out,PT}}{P_{in,PT}}$$

$$\eta_{m,PT} = \frac{32.70 \text{watts}}{95.87 \text{ watts}} = .338$$

$$T_{PTi} (Nm) = I * t_c$$

$$T_{PTi} (Nm) = 7.64 \text{amps} * .11 \left(\frac{Nm}{A} \right) = .8404 Nm$$

$$T_{PTo} (Nm) = T_{PTi} - T_f$$

$$T_{PTo} (Nm) = .8404 Nm - .12 Nm = .7204 Nm$$

$$P_{out,PT2} (W) = T_{out,PT2} * S$$

$$P_{out,PT2} (W) = .7204 Nm * 76.45 \frac{rad}{sec} = 55.07 W$$

$$\eta_{m,PT2} = \frac{P_{out,PT2}}{P_{in,PT}}$$

$$\eta_{m,PT2} = \frac{55.07 W}{95.87 W} = .574$$

BAS :

$$P_{LM,o} (W) = VI$$

$$P_{LM,o} (W) = 7.62V * 1.54amps = 11.73 \text{ watts}$$

$$T_{LM,i} (Nm) = I * t_c + t_f$$

$$T_{LM,i} (Nm) = 1.54amps * \frac{11Nm}{amp} + .12Nm = .2894Nm$$

$$\omega \left(\frac{r}{s} \right) = \frac{2\pi}{60} * s$$

$$\omega \left(\frac{r}{s} \right) = \frac{2\pi}{60} * 730RPM = 76.45 \frac{r}{s}$$

$$P_{LM,i} (W) = T_{LM,i} * \omega$$

$$P_{LM,i} (W) = .2894Nm * \frac{76.45r}{s} = 22.12 W$$

$$\eta_{LM} = \frac{P_{LM,o}}{P_{LM,i}}$$

$$\eta_{LM} = \frac{11.73W}{22.12W} = .530$$

Front Load Axle:

$$P_{LM,o} (W) = VI$$

$$P_{LM,o} (W) = 7.29V * 1.55amps = 11.30 \text{ watts}$$

$$T_{LM,i} (Nm) = I * t_c + t_f$$

$$T_{LM,i} (Nm) = 1.55amps * \frac{11Nm}{amp} + .12Nm = .2905Nm$$

$$\omega \left(\frac{r}{s} \right) = \frac{2\pi}{60} * s$$

$$\omega \left(\frac{r}{s} \right) = \frac{2\pi}{60} * 730RPM = 76.45 \frac{r}{s}$$

$$P_{LM,i} (W) = T_{LM,i} * \omega$$

$$P_{LM,i} (W) = .2905Nm * \frac{76.45r}{s} = 22.09 W$$

$$\eta_{LM} = \frac{P_{LM,o}}{P_{LM,i}}$$

$$\eta_{LM} = \frac{11.30W}{22.09W} = .512$$

Overall Axle Efficiency:

$$\eta_{axle} = \frac{\Sigma((V * I)_{resistor})}{(V * I)_{battery}} = \frac{\Sigma(P_{resistor})}{P_{battery}}$$

$$\eta_{axle} = \frac{\Sigma((V*I)_{resistor})}{(V*I)_{battery}} = \frac{\Sigma(11.30+11.73 W)}{95.87W} = .240$$